

UNCLASSIFIED  
~~CONFIDENTIAL~~

NASA TECHNICAL  
MEMORANDUM



NASA TM X-1008

C.2

CLASSIFICATION CHANGED

To UNCLASSIFIED

LIBRARY COPY

By authority of *ASTAR* Date *12-31-70* SEP 18 1964  
*V.8, No.24* *Bern*

*3-18-71*

LANGLEY RESEARCH CENTER  
LIBRARY, NASA  
LANGLEY STATION  
HAMPTON, VIRGINIA

TRANSONIC CHARACTERISTICS OF  
A HYDROGEN-FUELED MULTISTAGE  
HORIZONTAL-TAKE-OFF  
REUSABLE LAUNCH VEHICLE

*by Larry R. Clark and P. Kenneth Pierpont*

*Langley Research Center*

*Langley Station, Hampton, Va.*

~~CONFIDENTIAL~~  
UNCLASSIFIED

NASA TM X-1008

UNCLASSIFIED  
~~CONFIDENTIAL~~

CLASSIFICATION CHANGED

To UNCLASSIFIED

By authority of STAR Date 12-31-70  
V.8 No. 24 Blm  
3-18-71

TRANSONIC CHARACTERISTICS OF A

HYDROGEN-FUELED MULTISTAGE HORIZONTAL-TAKE-OFF

REUSABLE LAUNCH VEHICLE

By Larry R. Clark and P. Kenneth Pierpont

Langley Research Center  
Langley Station, Hampton, Va.

GROUP 4  
Downgraded at 3 year intervals;  
declassified after 12 years

CLASSIFIED DOCUMENT—TITLE UNCLASSIFIED

This material contains information affecting the national defense of the United States within the meaning of the espionage laws, Title 18, U.S.C., Secs. 793 and 794, the transmission or revelation of which in any manner to an unauthorized person is prohibited by law.

NATIONAL AERONAUTICS AND SPACE ADMINISTRATION

UNCLASSIFIED  
~~CONFIDENTIAL~~

~~CONFIDENTIAL~~  
UNCLASSIFIED

TRANSONIC CHARACTERISTICS OF A  
HYDROGEN-FUELED MULTISTAGE HORIZONTAL-TAKE-OFF  
REUSABLE LAUNCH VEHICLE\*

By Larry R. Clark and P. Kenneth Pierpont  
Langley Research Center

SUMMARY

A wind-tunnel investigation was made at subsonic and transonic speeds of an approximate 1/75-scale model of a multistage horizontal-take-off reusable launch vehicle. The model consisted of a winged reusable first stage, a winged reusable second stage, and a third-stage winged reusable spacecraft with an expendable maneuvering propulsion package. The two upper stages were arranged in tandem, and this combination was placed parallel to the first-stage reusable booster. The model was tested at Mach numbers from 0.6 to 1.2, angles of attack up to about  $32^\circ$ , and generally at sideslip angles of  $0^\circ$  and  $5^\circ$ . The test Reynolds numbers per foot varied from approximately  $3.3 \times 10^6$  to  $4.2 \times 10^6$ .

The first-stage reusable booster and its several modifications were all longitudinally stable at zero lift for the selected moment reference center. The complete first stage was directionally stable and had positive effective dihedral over the entire Mach number range and most of the angle-of-attack range of these tests. The canard was very destabilizing longitudinally, but increased effective dihedral and directional stability significantly at high angles of attack. The maximum lift-drag ratios for the complete first stage varied between about 3.8 and 4.7 over the test Mach number range.

The addition of the complete upper stages to the complete first stage caused destabilizing increments both longitudinally and directionally, and caused some reductions in positive effective dihedral. In general, the complete launch vehicle and its several variations were longitudinally stable at zero lift and had positive effective dihedral, but were generally directionally unstable for the selected moment reference center.

INTRODUCTION

A program of investigation is being conducted at the Langley Research Center to study some of the aerodynamic problems associated with horizontal-take-off and vertical-take-off reusable orbital launch vehicles. Data are

---

\*Title, Unclassified.

~~CONFIDENTIAL~~  
UNCLASSIFIED

~~CONFIDENTIAL~~  
UNCLASSIFIED

available for several configurations in references 1 to 5. The present tests are a continuation of the study of the horizontal-take-off reusable launch vehicle concept and provide data for a hydrogen-fueled design in the subsonic and transonic speed ranges.

The launch vehicle consisted of a winged reusable first stage, a winged reusable second stage, and a third-stage winged reusable spacecraft with an expendable space-maneuvering propulsion package. The two upper stages were arranged in tandem, and this combination was placed parallel to the first-stage reusable booster. The first-stage reusable booster consisted of a large volume fuselage with a delta wing and canard and vertical fins mounted outboard on the wing. The second-stage reusable booster consisted of a cylindrical fuselage with a trapezoidal wing and outboard-mounted vertical fins. The spacecraft employed a clipped delta wing with toed-in tip-mounted vertical fins and a cylindrical, expendable, space-maneuvering propulsion package.

All stages of the vehicle were conceived to employ rocket engines using liquid oxygen and hydrogen propellants during boost. The first-stage reusable booster was considered to utilize turbojet engines for its return flight, whereas the second-stage reusable booster was conceived to be a glide return vehicle. The launch vehicle was designed to place a maximum of 20,000 pounds into earth orbit. Stage separation was estimated to occur at a speed of 6500 fps at about 230,000 feet altitude, and the take-off wing loading was assumed to be 120 lb/sq ft, based on total wing area.

Tests were conducted on a 1/75-scale model in the Langley 8-foot transonic pressure tunnel at Mach numbers from 0.6 to 1.2, angles of attack up to about  $32^\circ$ , and generally at angles of sideslip of  $0^\circ$  and  $5^\circ$ . The Reynolds numbers per foot varied from approximately  $3.3 \times 10^6$  to  $4.2 \times 10^6$ .

#### SYMBOLS

Longitudinal force and moment coefficients were referred to the stability axes and the lateral and directional force and moment coefficients were referred to the body axes. The moment reference center was located at 15 percent of the mean aerodynamic chord of the first-stage wing, in the upper surface of the wing, and was 12.47 inches forward of the model base. All aerodynamic coefficients are based on the geometry of the wing of the first-stage reusable booster.

$C_L$  lift coefficient,  $\frac{\text{Lift}}{qS}$

$C_{L,(L/D)_{\max}}$  lift coefficient at maximum lift-drag ratio

$C_D$  drag coefficient,  $\frac{\text{Drag}}{qS}$

~~CONFIDENTIAL~~  
UNCLASSIFIED

~~CONFIDENTIAL~~  
UNCLASSIFIED

$C_m$	pitching-moment coefficient, $\frac{\text{Pitching moment}}{qS\bar{c}}$
$C_l$	rolling-moment coefficient, $\frac{\text{Rolling moment}}{qSb}$
$C_n$	yawing-moment coefficient, $\frac{\text{Yawing moment}}{qSb}$
$C_Y$	side-force coefficient, $\frac{\text{Side force}}{qS}$
$C_{L_\alpha}$	lift-curve slope (at zero lift), $\frac{\partial C_L}{\partial \alpha}$ , per deg
$C_{mC_L}$	longitudinal-stability parameter (at zero lift), $\frac{\partial C_m}{\partial C_L}$
$C_{m\delta}$	control effectiveness of canard, $\frac{\Delta C_m}{\Delta \delta}$ , per deg
$\frac{\partial C_D}{\partial C_L^2}$	drag-due-to-lift factor
$C_{l\beta}$	effective-dihedral parameter, $\frac{\Delta C_l}{\Delta \beta}$ , per deg
$C_{n\beta}$	directional-stability parameter, $\frac{\Delta C_n}{\Delta \beta}$ , per deg
$C_{Y\beta}$	side-force parameter, $\frac{\Delta C_Y}{\Delta \beta}$ , per deg
$L/D$	lift-drag ratio, $\frac{C_L}{C_D}$
$b$	reference wing span, 1.333 ft
$c$	local chord, ft
$\bar{c}$	reference mean aerodynamic chord, based on total wing area, 1.222 ft
$M$	free-stream Mach number

~~CONFIDENTIAL~~  
UNCLASSIFIED

UNCLASSIFIED

q free-stream dynamic pressure, lb/sq ft  
R Reynolds number per foot  
S reference wing area, 1.222 sq ft  
 $\alpha$  angle of attack, deg  
 $\beta$  angle of sideslip, deg  
 $\delta$  angle of canard deflection (positive for leading edge up), deg

Subscripts:

o conditions at zero lift  
max maximum

Component designations:

B fuselage, first- or second-stage  
B' fuselage, second-stage with an afterbody fairing  
W wing, first- or second-stage  
C canard,  $\delta = 0^\circ$   
C' canard,  $\delta = -5^\circ$   
N nacelles, first-stage  
F vertical fins, first- or second-stage  
M maneuver propulsion package  
S spacecraft with mounting pad

DESCRIPTION OF MODEL

The complete launch vehicle and its components are shown in figure 1. The launch vehicle consisted of a winged reusable first stage, a winged reusable second stage, and a third-stage winged reusable spacecraft with an expendable space-maneuvering propulsion package. The two upper stages were arranged in tandem, and this combination was placed parallel to the first-stage reusable booster. Principal model dimensions are presented in table I and photographs of the model are shown in figure 2.

UNCLASSIFIED

UNCLASSIFIED

### First-Stage Reusable Booster

The first-stage reusable booster consisted of a semicylindrical fuselage with an ogival forebody, a delta canard, and a delta wing with outboard trapezoidal vertical fins mounted on nacelles (fig. 1(b)). The semicylindrical portion of the fuselage was 5 diameters long and the ogive nose (or forebody) was  $4\frac{1}{2}$  diameters long. The canard had a delta planform with  $70^\circ$  of leading-edge sweep and a wedge-slab symmetrical airfoil with 0.05c maximum thickness (fig. 1(d)). The canard had a constant leading-edge radius of about 0.04 inch. The exposed area of the canard was about 7 percent of the total first-stage wing area, and the distance between 0.25c of the canard and 0.25c of the first-stage wing was 1.4c of the wing. Provision was made for testing the canard at  $0^\circ$  and  $-5^\circ$ . The wing had  $70^\circ$  of leading-edge sweep and was a symmetrical wedge to the 40-percent-chord station with a constant 0.050c maximum thickness rearward to the 0.85c station. A wedge or boattail on the lower surface of the wing extended from 0.85c to the wing trailing edge. (See fig. 1(c)). The first-stage wing had a constant leading-edge radius of 0.04 inch, which was the same as for most aerodynamic surfaces of the vehicle, and the wing was flat on the upper surface rearward of the 40-percent station to allow mating with the second-stage wing. The requirement for a flat upper surface resulted in a wing dihedral angle of about  $3\frac{1}{2}^\circ$ . The vertical fins had  $60^\circ$  of leading-edge sweep and simple wedge airfoils with the maximum thickness of 0.05c at the base. The fins were located outboard at two-thirds of the wing semispan, and the total fin area, which was equally distributed above and below the wing, was approximately 15 percent of the total wing area. The vertical fins had an aspect ratio of 1.15 and a taper ratio of 0.5. The nacelles were cylindrical with a parabolic nose and were considered to house the flyback engines. The nacelles formed the juncture between the first-stage wing and vertical fins.

### Second-Stage Reusable Booster

The second-stage reusable booster consisted of a cylindrical fuselage  $7\frac{1}{2}$  diameters long (including a conceived nose design 1 diameter in length) and a trapezoidal wing with two outboard-mounted vertical fins located at two-thirds of the semispan of the wing. The fuselage incorporated a side fairing which extended vertically from the center line of the second-stage fuselage to the upper surface of the first-stage fuselage. The wing had  $58.75^\circ$  of leading-edge sweep and a 0.028c maximum thickness. The wing thickness was chosen to achieve a total profile thickness of 0.065c (based on the chord of the first-stage wing) when the first- and second-stage wings were mated. The upper surface of the second-stage wing was an extension of the upper wedge surface of the first-stage wing; that is, the two upper wedge surfaces were coplanar. A portion of the leading edge of this extension was removed to form a constant leading-edge radius on the second-stage wing identical to that of the first-stage wing. The purpose of this arrangement was to reduce the interference of the mated wings during launch. The second-stage vertical fins were almost identical to the first-stage vertical fins, but only the upper element was employed.

UNCLASSIFIED

~~CONFIDENTIAL~~  
UNCLASSIFIED

## Orbital Stage

The spacecraft was a wing-body configuration with toed-in, wing-tip-mounted, vertical fins (fig. 1(d)). The spacecraft wing was unsymmetrical with the camber adjacent to the fuselage and the span (including vertical fins) was approximately equal to the width of the first-stage fuselage. The wing had  $72.5^\circ$  of leading-edge sweep and 0.05c maximum thickness. The wing had a constant leading-edge radius of 0.04 inch. The vertical fins were trapezoidal with  $55^\circ$  of leading-edge sweep and 0.05c maximum thickness. The leading-edge radius of the fins is 0.04 inch - the same as that for the wing.

The maneuver propulsion package was an expendable rocket booster which was 3 diameters long, including the spacecraft adapter fairing. It was a short cylinder with the same diameter as the second-stage fuselage and also incorporated the same type of side fairing as the second-stage fuselage. When the model was tested without the maneuver propulsion package, the spacecraft was moved rearward to connect directly with the second-stage fuselage.

## APPARATUS AND TESTS

The several model configurations were sting mounted in the wind tunnel on a six-component strain-gage balance. Boundary-layer transition was fixed on the model with a 0.1-inch-wide strip of No. 80 carborundum (0.008-inch-diameter grains) located at the 5-percent station on all surfaces. The angles of attack and sideslip were corrected for balance and sting deflections under load. The balance chamber pressure and the first-stage fuselage base pressure were measured for use in base-drag correction. Except where noted, the drag of the vehicle was corrected to correspond to a base pressure equal to the free-stream static pressure on the first-stage reusable booster fuselage and that portion of the first-stage wing base intercepted by the fuselage. No pressure corrections were applied to the base area of the second-stage booster.

The tests were conducted in the Langley 8-foot transonic pressure tunnel at Mach numbers from 0.6 to 1.2, angles of attack up to about  $32^\circ$ , and generally at angles of sideslip of  $0^\circ$  and  $5^\circ$ . The Reynolds numbers per foot are shown in figure 3 to vary from approximately  $3.3 \times 10^6$  to  $4.2 \times 10^6$ .

## PRESENTATION OF RESULTS

The basic longitudinal aerodynamic characteristics (figs. 4 to 8) have been summarized for comparison in figures 9 to 12. In addition, the basic lateral aerodynamic characteristics (figs. 13 to 15) have been presented for analysis in figures 16, 17, and 18. In the following figures, the several configurations were identified with letter symbols for purposes of clarification. (See symbol list for component identification.)

~~CONFIDENTIAL~~  
UNCLASSIFIED

Longitudinal aerodynamic characteristics at $\beta = 0^\circ$ for:	
First-stage fuselage . . . . .	4
First-stage reusable booster with the effects of the canard, nacelles, and vertical fins . . . . .	5
First-stage reusable booster with the canard at $0^\circ$ and $-5^\circ$ deflection . . . . .	6
Launch vehicle with the effects of the first- and second-stage vertical fins and the second-stage wing . . . . .	7
Launch vehicle with the effects of a second-stage afterbody fairing, the maneuver propulsion package, and a canard deflection of $-5^\circ$ . . . . .	8
The variation with Mach number at $\beta = 0^\circ$ of:	
Lift-curve slopes for several first-stage and launch configurations . . . . .	9
Longitudinal-stability parameters for several first-stage and launch configurations and the canard effectiveness for a first-stage and a launch configuration . . . . .	10
Drag-at-zero-lift and drag-due-to-lift parameters for several first- stage and launch configurations . . . . .	11
Maximum lift-drag ratio and the lift coefficient at which the maximum lift-drag ratio occurs for several first-stage and launch configurations . . . . .	12
Lateral aerodynamic characteristics for:	
Several first-stage configurations at $\beta = 0^\circ$ and $5^\circ$ . . . . .	13
First-stage reusable booster at $\alpha = 10^\circ$ for a $\beta$ -range . . . . .	14
Several launch configurations at $\beta = 0^\circ$ and $5^\circ$ . . . . .	15
The variation with angle of attack of the lateral- and directional- stability parameters for the complete first stage and the complete launch vehicle . . . . .	
	16
The variation with Mach number at $\alpha = 0^\circ$ , $6^\circ$ , and $12^\circ$ of:	
Lateral-stability parameters for several first-stage and launch configurations . . . . .	17
Directional-stability parameters for several first-stage and launch configurations . . . . .	18
Side-force parameters for several first-stage and launch configurations . . . . .	19

## DISCUSSION OF RESULTS

The discussion will indicate some of the effects of the various components and stages on the aerodynamic characteristics of the first-stage reusable booster and the basic take-off launch vehicle.

UNCLASSIFIED

## Lift Characteristics

First-stage reusable booster.- The first-stage reusable booster and its several variations, except the first-stage fuselage alone, had considerable negative lift at zero angle of attack for all test Mach numbers. (See figs. 4, 5(a), and 6(a).) The negative lift at zero angle of attack observed is considered to have been caused primarily by a negative camber effect of a boattail on the lower surface of the wing which extended rearward from the 0.85c station to the wing trailing edge. Further discussion of this camber effect is presented in the section on longitudinal stability. The boattail was incorporated in the wing design to reduce the wing base drag while providing a flat upper surface for a flush mating with the second-stage wing.

Figure 6(a) shows that  $C_{L,max}$  was not obtained for the complete first stage at any of the test Mach numbers although the tests included angles up to about  $32^\circ$ . The usual decrease in  $C_{L\alpha}$  occurred as angles of attack increased beyond about  $15^\circ$ .

Figure 9 shows the expected  $C_{L\alpha}$  increases with Mach number for the complete first stage to be about 10 percent and the variations in  $C_{L\alpha}$  with Mach number were similar for all configurations. The magnitudes of  $C_{L\alpha}$  for the first stage without the canard over the Mach number range were approximately the same as those values for the reusable booster of reference 1, but as much as 40 percent lower than the  $C_{L\alpha}$  values for the reusable booster in reference 2. When proper account is taken of the differences in the ratio of exposed area to the total wing area of the three vehicles, the  $C_{L\alpha}$  values shown for the present first stage are compatible with those for the reference vehicles.

The values of  $C_{L\alpha}$  for the complete first stage were reduced as much as 9 percent as a result of removing the first-stage fins and nacelles. This was probably caused by the end-plate effect of the vertical fins which would be expected to reduce the outboard component of local flow, thereby effectively increasing the wing loading. The canard had a negligible effect on  $C_{L\alpha}$ , even though the exposed area of the canard was approximately 7 percent of the total first-stage wing area. The negligible effect of the canard on  $C_{L\alpha}$  apparently resulted from a reduction in lift on the first-stage wing caused primarily by downwash from the canard on the inboard portion of the wing near the fuselage which nullified any increased lift generated on the canard. A trapezoidal-canard delta-wing configuration in reference 6 showed a similar behavior.

Launch vehicle.- In general, the complete upper stages were responsible for small increases in lift at zero angle of attack at all of the test Mach numbers (figs. 5(a), 7(a), and 8(a)). These increases in lift at zero angle of attack resulted from the effective change in the first-stage wing profile caused by mating the first- and second-stage wings. Replacing the cylindrical second-stage afterbody with the curved boattail fairing (fig. 1) produced sizable increases in lift at zero angle of attack. This suggests that appreciable

UNCLASSIFIED

UNCLASSIFIED

~~CONFIDENTIAL~~

negative local static pressures occurred near the shoulder of the fairing and on the local wing surface nearby. The negative pressures were caused by the expected acceleration of the flow around the shoulder of the fairing which would then be followed by a recompression toward the rear end of the fairing.

The addition of the complete upper stages to the first stage caused some small reductions in  $C_{L\alpha}$  at all test Mach numbers. These decreases are attributed to the blockage of the upper stages which reduced the carryover lift from the first-stage wing on the first-stage fuselage. These losses are not too important, however, since the launch vehicle is to be rocket powered. Figure 9 shows that there were only small variations in  $C_{L\alpha}$  as a result of changes made in the complete launch vehicle.

### Longitudinal-Stability Characteristics

First-stage reusable booster.- Figure 5(b) shows that the complete first stage and its several modifications exhibited large positive  $C_{m,0}$  values at all test Mach numbers. Comparison of the canard-on and canard-off data indicates that the canard was not in itself responsible for the large positive  $C_{m,0}$  values observed. Also, figure 4 indicates that the body alone contributed very little pitching moment at zero lift. The boattail on the lower surface of the wing near its trailing edge was primarily responsible for the large positive  $C_{m,0}$  values observed. At  $M = 0.9$ , the center of pressure at  $\alpha = 0^\circ$  was calculated for the wing-fuselage configuration and was found to act at approximately 1.15 inches forward of the wing base. This would place the center of pressure at the boattail and indicates that the boattail was probably responsible for the negative lift and the positive  $C_{m,0}$  values for the first-stage vehicles.

Figure 10 shows that the complete first stage and its several variations all had some longitudinal stability at  $C_L = 0$  for the chosen moment reference center of  $0.15\bar{c}$ . However, figure 5(b) shows the pitching-moment curves to be nonlinear with some instability for all the configurations over some portion of the lift range. The canard made a very large destabilizing contribution to longitudinal stability, but the first-stage fins and nacelles were slightly stabilizing which would follow logically from their end-plate effect.

The control effectiveness of the canard is shown in figure 10 for the complete first stage. Values of  $C_{m\delta}$  increased with lift coefficient to give values of  $C_{m\delta}$  at  $C_L = 0.4$  about double the values at  $C_L = 0$ . The high positive  $C_{m,0}$  values for the first stage necessitated the negative deflection of the canard in an attempt to trim the vehicle. Since it is considered that the canard will be needed to provide control during reentry of the first stage, higher  $L/D$  values and better trim control might be obtained by incorporating trailing-edge flaps for control at subsonic and transonic speeds and employing a free-floating canard at subsonic speeds, but a rigid canard to provide the necessary control at supersonic speeds.

~~CONFIDENTIAL~~  
UNCLASSIFIED

Launch vehicle.- The addition of the upper stages to the first stage to form configuration (BWNCF + BWFMS) produced a small decrease in  $C_{m,o}$ . This was caused by the addition of the second-stage wing which changed the effective camber of the first-stage wing when the two wings were mated. Also, the upper-wedge surface, or boattail, at the rear of the second-stage wing should have produced some increased lift. The combination of these factors resulted in a  $C_{m,o}$  decrease of as much as 0.026 when the second-stage wing was added. The addition of the second-stage afterbody fairing caused large decreases in  $C_{m,o}$  at all test Mach numbers. This effect would follow logically because of its lift characteristics, as discussed previously.

The addition of the complete upper stages to the complete first stage had little effect on the longitudinal stability of the first stage at any of the test Mach numbers (fig. 10). The complete launch vehicle and all the configurations showing changes in the complete launch vehicle were longitudinally stable at zero lift, but they generally became unstable at high lift coefficients except at  $M = 1.03$  and 1.2. Only small changes in  $C_{mC_L}$  can be noted for changes in the launch configuration.

#### Drag and L/D Characteristics

First-stage reusable booster.- Figure 11 presents drag coefficients at zero lift for the complete first stage and indicates the magnitudes of the contributions of the canard and the nacelles and fins. Also shown in the figure is a curve of  $C_{D,o}$  for the complete first stage uncorrected for the fuselage base drag. Throughout the test Mach number range, this curve indicates values that were about 30 to 50 percent higher than those for the vehicle corrected for the base drag. Figure 11 reveals that, at  $M = 0.6$ , the fuselage base drag produced an increment in  $C_{D,o}$  of 0.007 whereas figure 4 shows that the first-stage fuselage, corrected for base drag, had a  $C_{D,o}$  value of only 0.006. Thus, the base drag exceeded the entire fuselage pressure and viscous drag. Not only was the fuselage base drag large, but pressures measured on the wing base and assumed to act also on the base of the nacelles and fins indicate that the base drag of these components at  $M = 0.6$  amounted to about 25 percent of the corrected  $C_{D,o}$  of the complete first stage.

Values of drag due to lift for the first-stage configurations varied between about 0.42 and 0.46 over the test Mach number range (fig. 11). In comparison with another delta-wing configuration,  $\frac{\partial C_D}{\partial C_L^2}$  values (drag-due-to-lift factor) for the present model were higher than those values for the first-stage reusable booster in reference 2. Reference 7 shows that  $\frac{\partial C_D}{\partial C_L^2}$  values for delta wings decrease with increases in Reynolds numbers based on the wing leading-edge radius. This decrease in drag-due-to-lift factor continues until the Reynolds number is high enough to achieve nearly full leading-edge suction,

UNCLASSIFIED

~~CONFIDENTIAL~~

after which no further decrease occurs. Drag-due-to-lift factors are shown in the reference to be most sensitive to leading-edge Reynolds number at subsonic speeds. The test Reynolds number of the present vehicle, based on leading-edge radius, indicated less than full leading-edge suction for the vehicle. Therefore, improvements in  $\frac{\partial C_D}{\partial C_L^2}$  at full-scale Reynolds numbers could be expected.

Figure 12 shows that, at  $M = 0.6$ , the first-stage wing-body combination had a maximum lift-drag ratio of 5.1, and the addition of the several components reduced  $(L/D)_{\max}$  to 4.7. Further reductions in  $(L/D)_{\max}$  to about 4.0 resulted from including base drag in the data. Throughout the test Mach number range,  $(L/D)_{\max}$  values for all the first-stage configurations, which were corrected for base drag, occurred between lift coefficients of about 0.20 and 0.32. The  $(L/D)_{\max}$  values presented for the complete first stage are relatively low for a vehicle which must function as an airplane with turbojet engines for its return flight. The actual return flight vehicle will have the detrimental base drag included, which is shown in figure 12 to yield values of  $(L/D)_{\max}$  between about 3.2 and 4.0 over the test Mach number range.

Launch vehicle. - The addition of the complete upper stages to the complete first stage caused increases in  $C_{D,0}$  of about 50 percent at all test Mach numbers (fig. 11). If this is important for a rocket-launch vehicle, ways of better integrating the upper stages with the first stage should be sought. None of the changes made in the basic launch configurations altered  $C_{D,0}$  values significantly. It was surprising that the increment in drag caused by the second-stage fins was so small since it would appear that their positioning on the vehicle would cause considerable interference on the other vehicle components.

An afterbody fairing placed at the rear of the main section of the second-stage fuselage had a negligible effect on  $C_{D,0}$  which resulted primarily from the negative local static pressures near the shoulder of the fairing caused by the acceleration of the flow around its curved surface. Figure 11 shows that the variations in  $C_{D,0}$  with Mach number were similar for all configurations. Drag-due-to-lift values for the launch configurations can be seen in figure 11 to be roughly the same as for the first-stage configurations.

The complete launch vehicle is shown in figure 12 to have maximum lift-drag ratios between about 2.9 and 4.0 which occurred at lift coefficients between approximately 0.28 and 0.40. These  $(L/D)_{\max}$  values are low, but since the launch vehicle will be rocket powered, high  $L/D$  values are not as important for the launch vehicle as for the first-stage reusable booster. The changes in  $(L/D)_{\max}$  caused by changes in the launch vehicle were small.

~~CONFIDENTIAL~~  
UNCLASSIFIED

## Lateral-Directional Characteristics

First-stage reusable booster.- Figure 16(a) shows that the complete first stage had positive effective dihedral (negative  $C_{l\beta}$ ) throughout the positive angle-of-attack range and Mach number range of these tests. In general, effective dihedral increased with angle of attack, but  $C_{l\beta}$  changed very little with increases in Mach number. Figure 17 shows data for several of the modifications of the first stage at  $\alpha = 0^\circ$ ,  $6^\circ$ , and  $12^\circ$ , which were considered a representative cross section of the data, and indicates that both the canard and the first-stage vertical fins had a significant favorable influence on effective dihedral at high angles of attack. Figure 14(a) shows rolling-moment coefficient plotted against sideslip angle at  $\alpha = 10^\circ$  for the complete first stage and shows the curves to be essentially linear between  $\beta = 0^\circ$  and  $5^\circ$  and to have only small deviations from linearity for the extreme sideslip-angle range.

The complete first stage was directionally stable at all test angles of attack and Mach numbers (fig. 16(b)). Figure 18 shows the effectiveness of the first-stage fins and the favorable influence of the canard on  $C_{n\beta}$  at  $\alpha = 0^\circ$ ,  $6^\circ$ , and  $12^\circ$  throughout the test Mach number range. In general, directional stability varied very little with Mach number. Figure 14(b) presents yawing-moment coefficients plotted against sideslip angle at  $\alpha = 10^\circ$  for the first stage. The curves are nonlinear between  $\beta = 0^\circ$  and  $5^\circ$ , but a linear curve could be reasonably approximated up to about  $6^\circ$ .

Launch vehicle.- The addition of the complete upper stages to the complete first stage caused sizable reductions in positive effective dihedral at all angles of attack throughout the test Mach number range (fig. 16(a)). Both the maneuver propulsion package and the second-stage fins resulted in some losses in effective dihedral indicating some interference on the load distribution of the wing (fig. 17). In general, effective dihedral increased with angle of attack, but changes in Mach number had little effect.

The addition of the complete upper stages to the complete first stage resulted in the launch vehicle which was directionally unstable (fig. 16(b)). The effectiveness of the first-stage fins was reduced by the blanketing effect of the upper stages, and probably some unfavorable side force ahead of the moment reference center contributed to the decrease in stability. Removal of the first-stage fins and nacelles decreased directional stability considerably, but the effect of the second-stage vertical fins was almost negligible (fig. 18). The removal of the maneuver propulsion package, accompanied by moving the spacecraft rearward, had a large favorable influence on stability resulting from the reduction of a sizable amount of side force on this component ahead of the moment reference center.

## SUMMARY OF RESULTS

An investigation has been made in the Langley 8-foot transonic pressure tunnel of a multistage horizontal-take-off reusable launch vehicle. The

~~CONFIDENTIAL~~  
UNCLASSIFIED

aerodynamic characteristics of the launch vehicle and the first-stage reusable booster with stage and component effects were determined at Mach numbers from 0.6 to 1.2, angles of attack up to about  $32^{\circ}$ , and generally at sideslip angles of  $0^{\circ}$  and  $5^{\circ}$ . The principal results may be summarized as follows:

1. The complete first-stage reusable booster was longitudinally stable at zero lift, directionally stable, and had positive effective dihedral over the entire Mach number and the positive angle-of-attack range of these tests for the selected moment reference center.
2. The canard produced large destabilizing increments longitudinally on the first-stage reusable booster, but increased effective dihedral and directional stability significantly at high angles of attack.
3. Maximum lift-drag ratios for the first-stage reusable booster varied between approximately 3.8 and 4.7 over the test Mach number range.
4. The addition of the complete upper stages to the complete first stage caused destabilizing increments both longitudinally and directionally, and caused some reductions in positive effective dihedral.
5. In general, the complete launch vehicle and its several variations were longitudinally stable and had positive effective dihedral, but were generally directionally unstable at all test Mach numbers.

Langley Research Center,  
National Aeronautics and Space Administration,  
Langley Station, Hampton, Va., April 4, 1964.

~~CONFIDENTIAL~~  
UNCLASSIFIED

UNCLASSIFIED

REFERENCES

1. Pierpont, P. Kenneth: Transonic Stability of a Preliminary Vertical-Take-Off Launch Configuration With a Horizontal-Landing Recoverable Booster. NASA TM X-689, 1962.
2. Pierpont, P. Kenneth: Transonic Longitudinal and Lateral Aerodynamic Characteristics of a Preliminary Concept of a First-Stage Horizontal-Take-Off-and-Horizontal-Landing Recoverable Booster With a 70° Delta Wing. NASA TM X-691, 1962.
3. Pierpont, P. Kenneth: Transonic Aerodynamic Characteristics of a Horizontal-Take-Off-and-Horizontal-Landing Recoverable-Booster Concept With Upper Stages Arranged in Parallel. NASA TM X-696, 1962.
4. Clark, Larry R., and Pierpont, P. Kenneth: Hypersonic Aerodynamic Characteristics of Preliminary Vertical-Take-Off Launch Configurations with a Horizontal-Landing Reusable Booster. NASA TM X-887, 1963.
5. Clark, Larry R., and Pierpont, P. Kenneth: Spacecraft and Stage-Geometry Effects on the Hypersonic Characteristics of a Horizontal-Take-Off Reusable Booster. NASA TM X-900, 1963.
6. Sleeman, William C., Jr.: Investigation at High Subsonic Speeds of the Static Longitudinal and Lateral Stability Characteristics of Two Canard Airplane Configurations. NACA RM L57J08, 1957.
7. Osborne, Robert S., and Kelly, Thomas C.: A Note on the Drag Due to Lift of Delta Wings at Mach Numbers Up to 2.0. NASA TN D-545, 1960. (Supersedes NACA RM L53A16a.)

UNCLASSIFIED

UNCLASSIFIED

TABLE I.- GEOMETRIC DESIGN CHARACTERISTICS OF THE MODEL

## First stage:

## Fuselage:

Length, in. . . . .	39.600
Maximum diameter, in. . . . .	4.206
Maximum height, in. . . . .	3.203
Nose radius, in. . . . .	0.160
Base area, sq in. . . . .	11.567

## Wing:

Total area, sq in. . . . .	176
Exposed area, sq in. . . . .	95.700
Span, in. . . . .	16
Root chord, in. . . . .	22
Tip chord, in. . . . .	0
Maximum thickness, percent chord . . . . .	5.000
Leading-edge sweep angle, deg . . . . .	70.00
Leading-edge radius, in. . . . .	0.040
Mean aerodynamic chord, in. . . . .	14.667
Moment reference center, percent $\bar{c}$ . . . . .	15
Moment reference center, in. from base . . . . .	12.467

## Vertical fins:

Area of each fin (exposed), sq in. . . . .	12.800
Height (exposed), in. . . . .	1.920
Root chord, in. . . . .	4.440
Tip chord, in. . . . .	2.220
Leading-edge sweep angle, deg . . . . .	60.00
Trailing-edge sweep angle, deg . . . . .	29.921
Leading-edge radius, in. . . . .	0.040

## Wing nacelles:

Length, in. . . . .	6.637
Maximum diameter, in. . . . .	0.960
Fineness ratio . . . . .	6.910
Nose radius, in. . . . .	0.160

## Canard:

Total area, sq in. . . . .	35.568
Exposed area, sq in. . . . .	12.440
Span, in. . . . .	7.200
Root chord, in. . . . .	9.880
Tip chord, in. . . . .	0
Maximum thickness, percent chord . . . . .	5
Leading-edge sweep angle, deg . . . . .	70.00
Leading-edge radius, in. . . . .	0.040

UNCLASSIFIED

UNCLASSIFIED

TABLE I.- GEOMETRIC DESIGN CHARACTERISTICS OF THE MODEL - Concluded

## Second stage:

## Fuselage:

Length, in. . . . .	16.000
Diameter, in. . . . .	2.134
Base area, sq in. . . . .	4.067

## Wing:

Total area, sq in. . . . .	75.200
Exposed area, sq in. . . . .	51.700
Span, in. . . . .	9.600
Root chord, in. . . . .	11.780
Tip chord, in. . . . .	3.852
Maximum thickness, percent chord . . . . .	2.800
Leading-edge sweep angle, deg . . . . .	58.75
Leading-edge radius, in. . . . .	0.040

## Vertical fins:

Area of each fin (exposed), sq in. . . . .	6.321
Height, in. . . . .	2.082
Root chord, in. . . . .	4.300
Tip chord, in. . . . .	2.220
Leading-edge sweep angle, deg . . . . .	60.00
Trailing-edge sweep angle, deg . . . . .	29.92
Leading-edge radius, in. . . . .	0.040

## Afterbody fairing:

Length, in. . . . .	7.233
Maximum diameter, in. . . . .	2.134

## Spacecraft:

## Fuselage:

Length, including interstage, in. . . . .	10.080
Diameter, in. . . . .	1.120
Interstage base diameter, in. . . . .	2.134
Interstage taper included angle, deg . . . . .	35.20
Length of nose cone, in. . . . .	1.428
Nose cone included angle, deg . . . . .	35.00
Nose radius, in. . . . .	0.160

## Wing:

Total area, sq in. . . . .	23.685
Exposed area, sq in. (top surface) . . . . .	14.852
Exposed area, sq in. (bottom surface) . . . . .	8.510
Span, in. . . . .	4.177
Root chord, in. . . . .	8.827
Tip chord, in. . . . .	2.648
Maximum thickness, percent chord . . . . .	5
Leading-edge sweep angle, deg . . . . .	72.50
Leading-edge radius, in. . . . .	0.040
Wing nose radius, in. . . . .	0.160

## Vertical fins:

Area, sq in. . . . .	2.405
Height, in. . . . .	1.430
Root chord, in. . . . .	2.648
Tip chord, in. . . . .	0.800
Maximum thickness, percent chord . . . . .	5
Leading-edge sweep angle, deg . . . . .	55.00
Leading-edge radius, in. . . . .	0.048
Toe-in angle, deg . . . . .	3.00

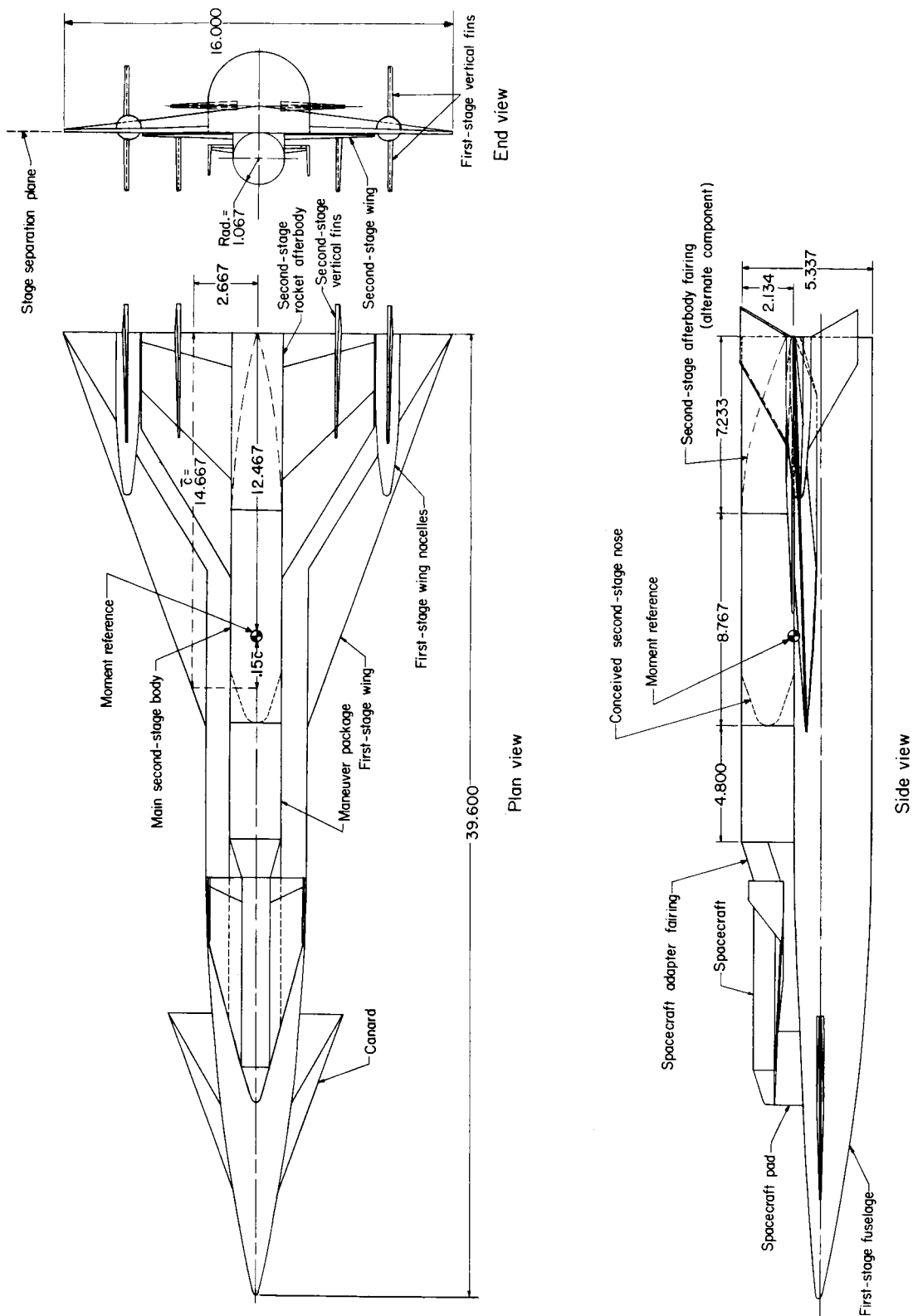
## Pad:

Length, in. . . . .	10.080
Maximum width, in. . . . .	2.134
Nose radius, in. . . . .	0.160
Wedge included angle, deg . . . . .	72.50

## Maneuver propulsion package:

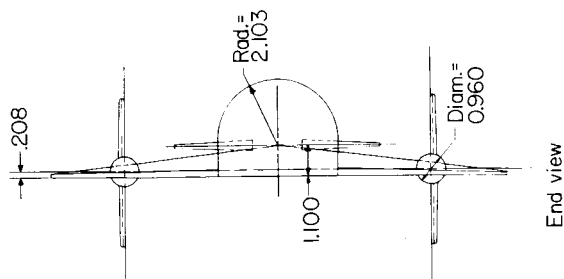
Length, in. . . . .	4.800
Diameter, in. . . . .	2.134

UNCLASSIFIED



(a) General arrangement of the launch vehicle.

Figure 1.- Arrangement and geometric details of a four-stage horizontal take-off reusable booster system. All linear design dimensions are in inches.

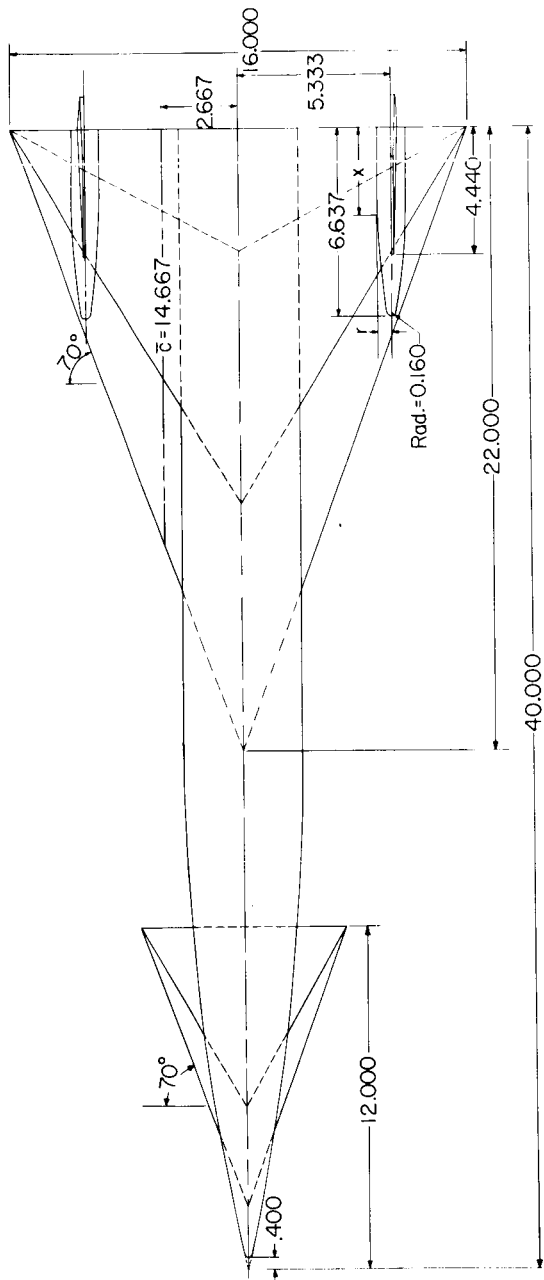


Wing nacelle coordinates

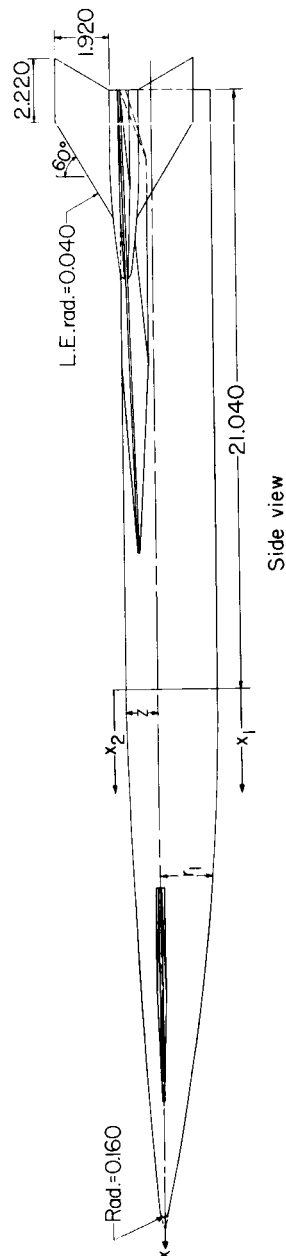
x	r
0	0.480
2.870	.480
3.703	.463
4.537	.412
5.370	.327

Fuselage coordinates

$x_1$	$x_2$	z
0	21.13	1.160
1.667	21.083	0.293
3.333	20.98	1.030
5.000	20.98	3.960
6.667	19.97	5.627
8.334	18.43	7.293
10.000	16.97	8.960
11.667	15.51	10.627
13.334	13.05	12.294
15.000	10.60	13.960
16.667	7.83	15.627
18.334	4.73	16.460
18.960	0	17.294
	.132	17.294
	18.127	230
	18.544	.163
	18.960	0



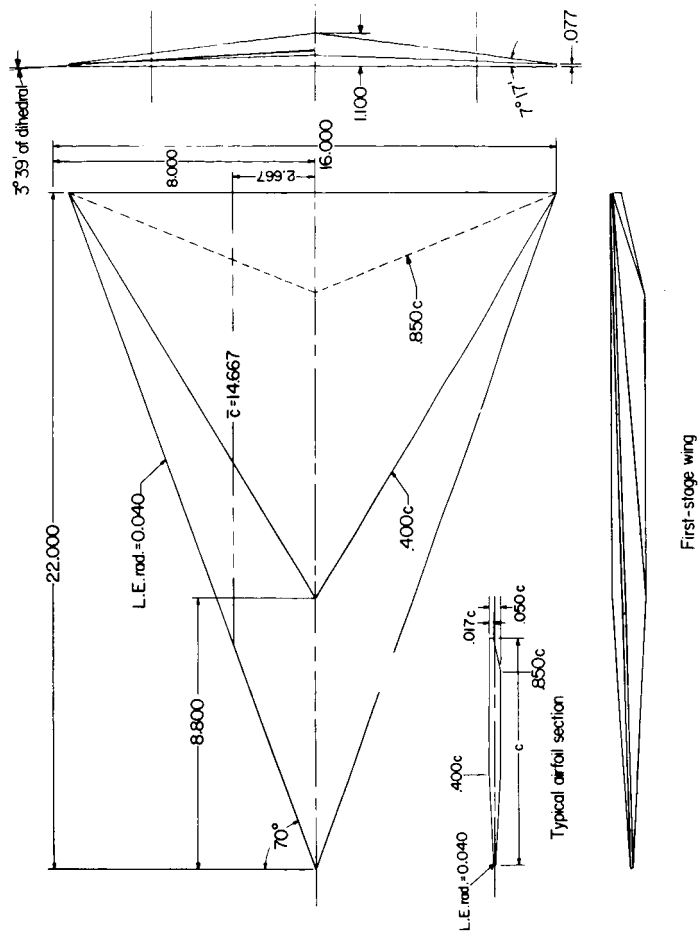
Plan view



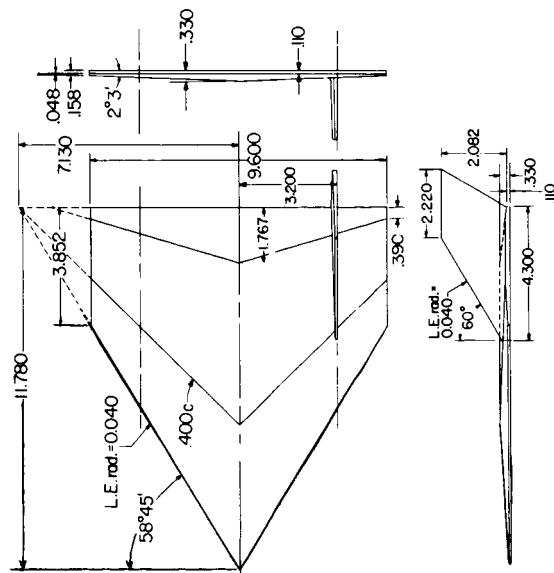
Side view

(b) First-stage reusable booster.

Figure 1.- Continued.



First-stage wing



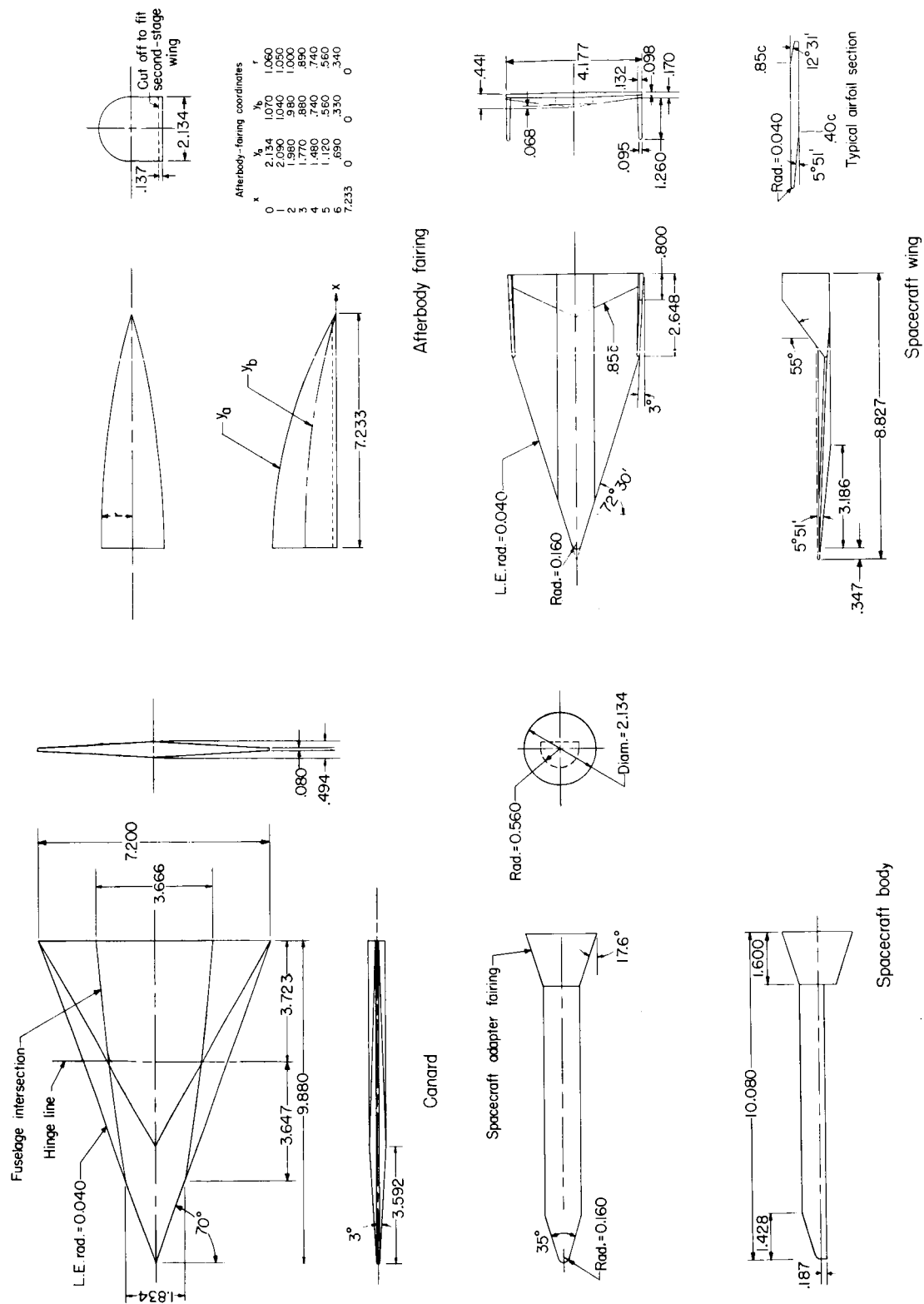
Second-stage wing

(c) Details of component parts.

Figure 1.- Continued.

~~CONFIDENTIAL~~

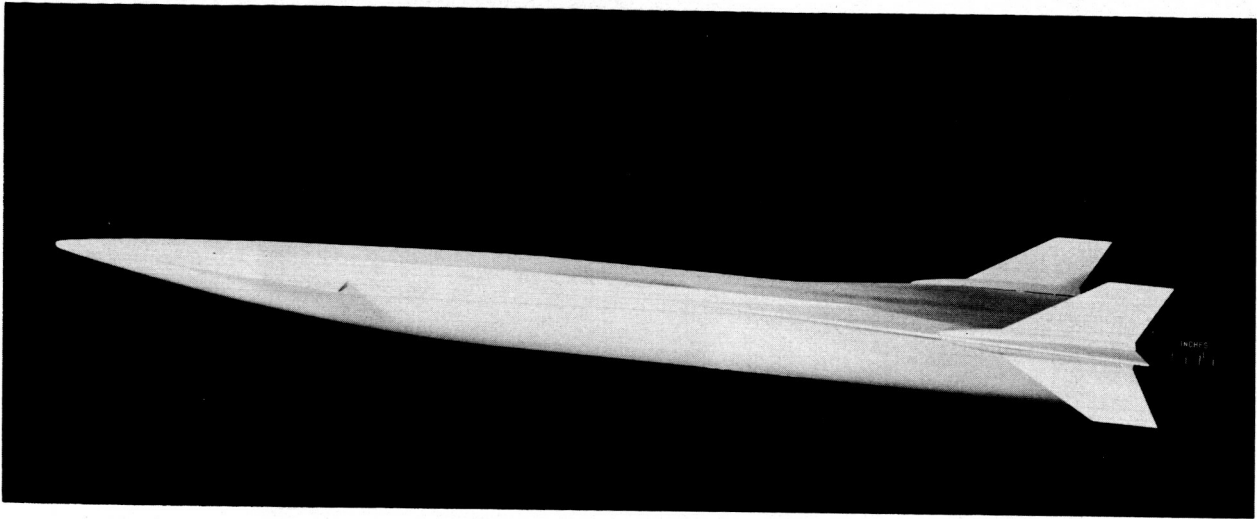
UNCLASSIFIED



(d) Details of component parts.

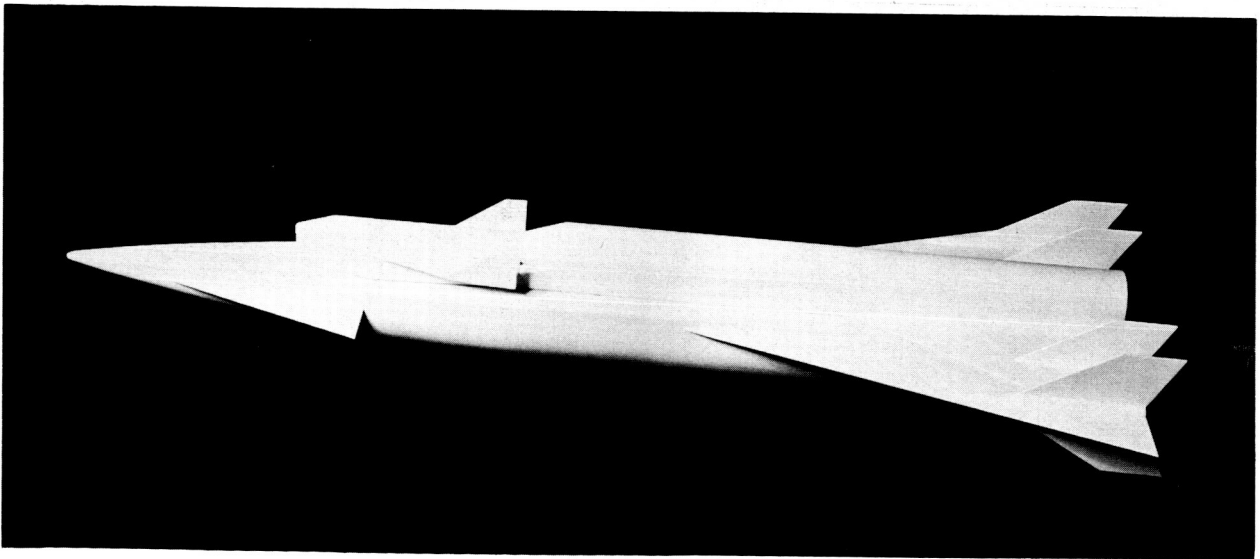
Figure 1.- Concluded.

UNCLASSIFIED



(a) First-stage reusable booster.

L-63-6483



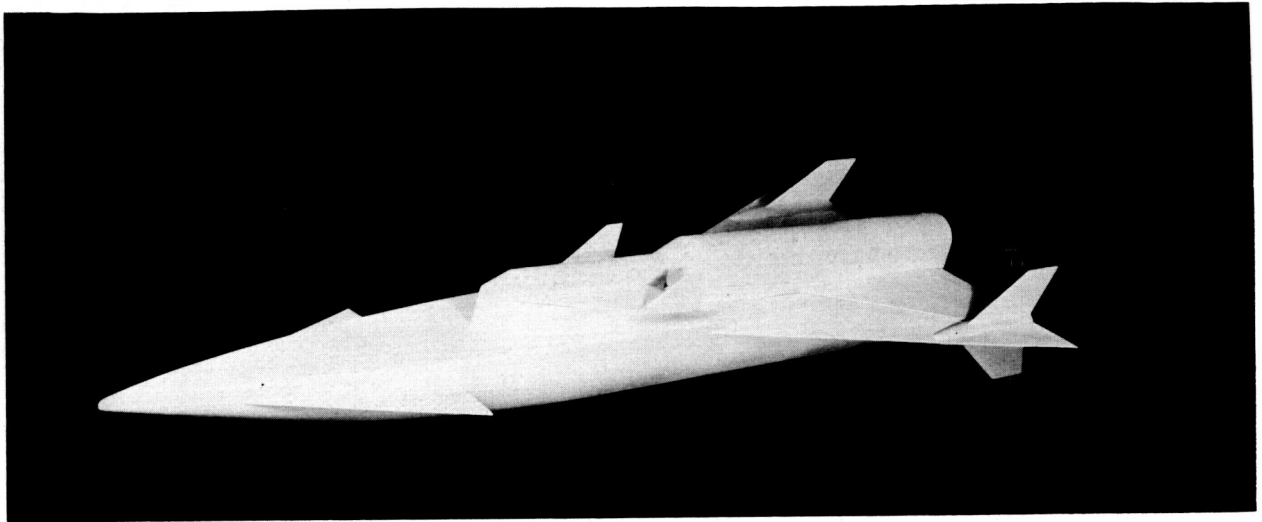
(b) Complete launch vehicle.

L-63-6490

Figure 2.- Photographs of model configurations.

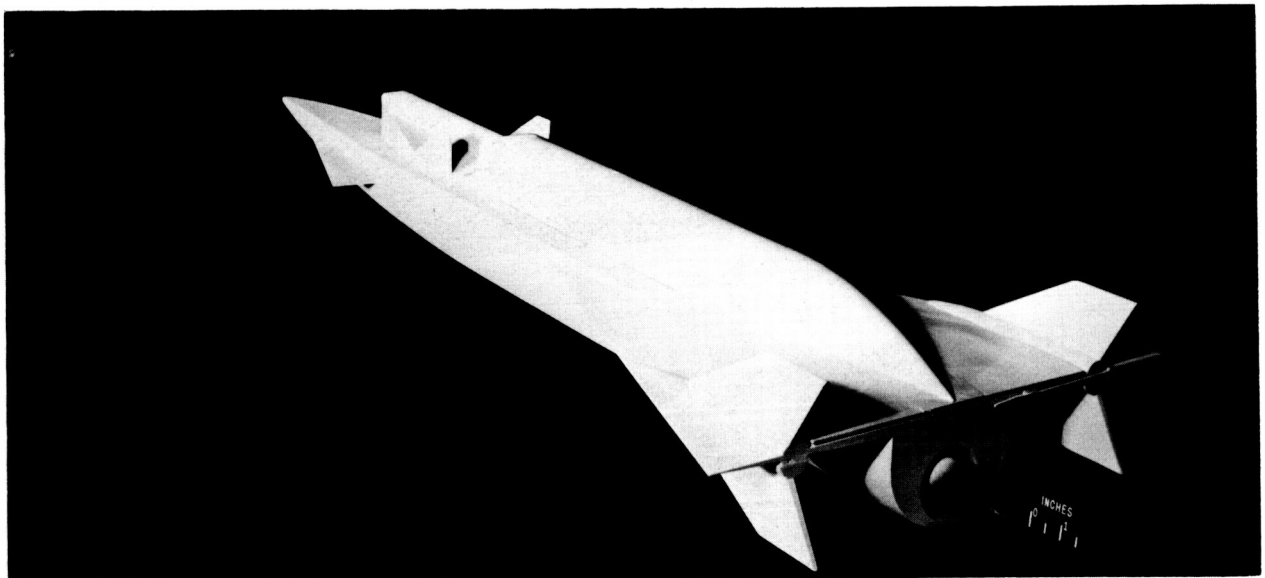
UNCLASSIFIED

~~CONFIDENTIAL~~  
UNCLASSIFIED



(c) Launch vehicle without the second-stage fins and maneuver stage.

L-63-6481



(d) Launch vehicle (without the second-stage fins) with a second-stage afterbody fairing.

L-63-6484

Figure 2.- Concluded.

~~CONFIDENTIAL~~  
UNCLASSIFIED

UNCLASSIFIED

~~CONFIDENTIAL~~

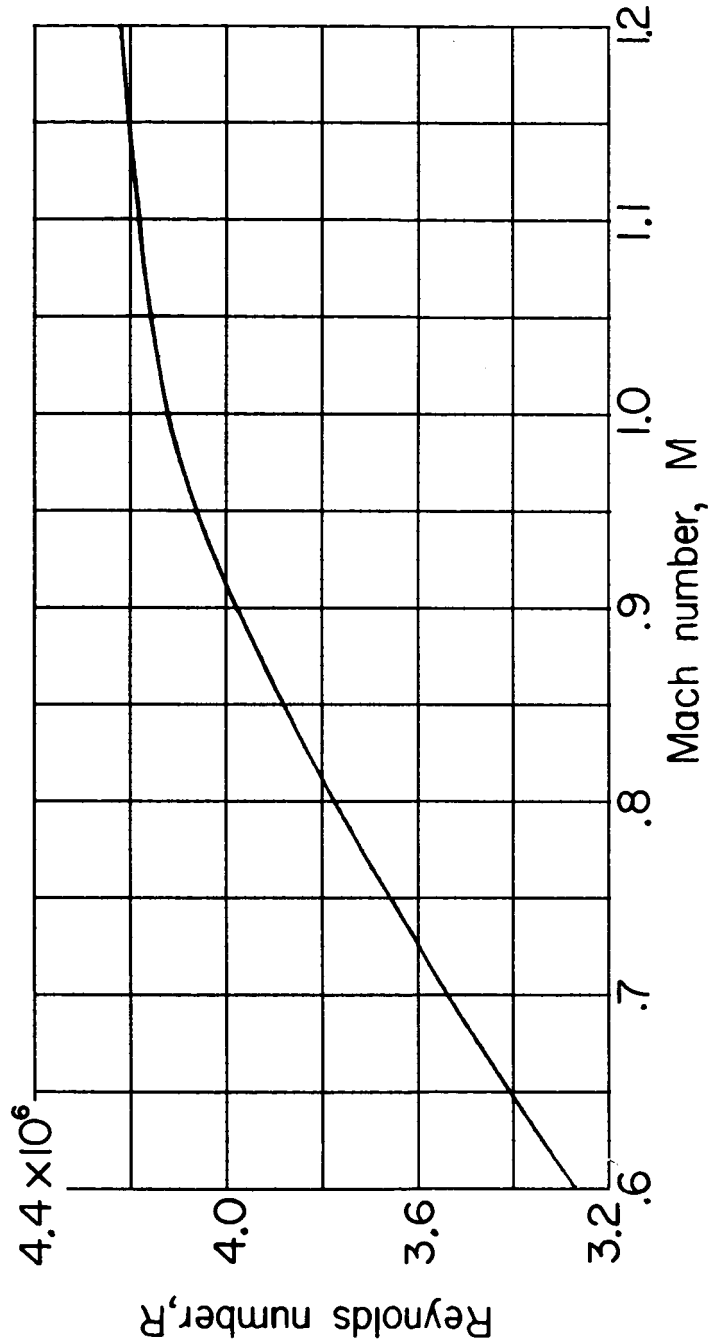


Figure 3.- Variation with Mach number of the test Reynolds number per foot.

~~CONFIDENTIAL~~

UNCLASSIFIED

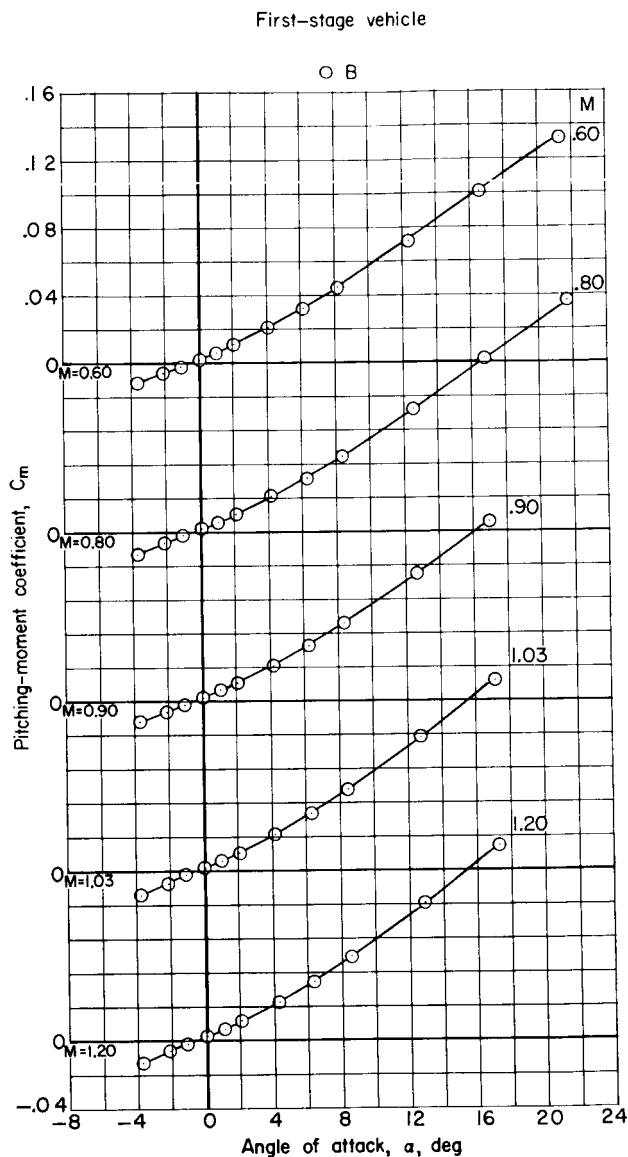
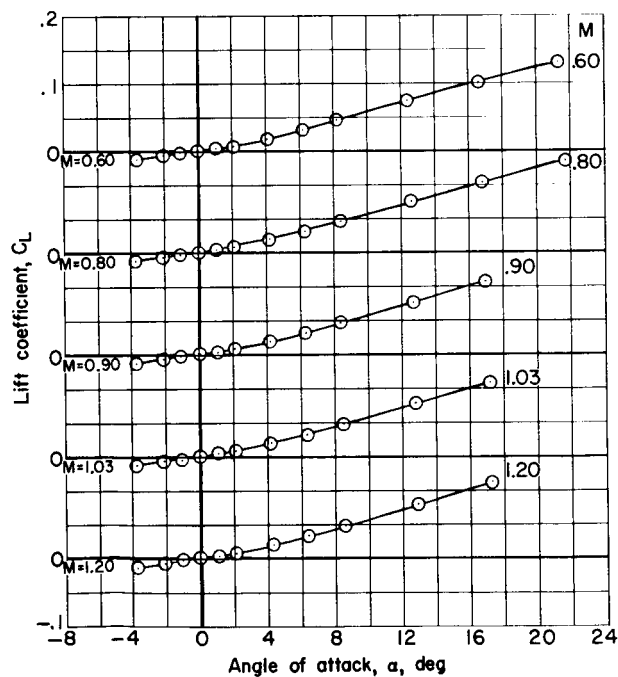
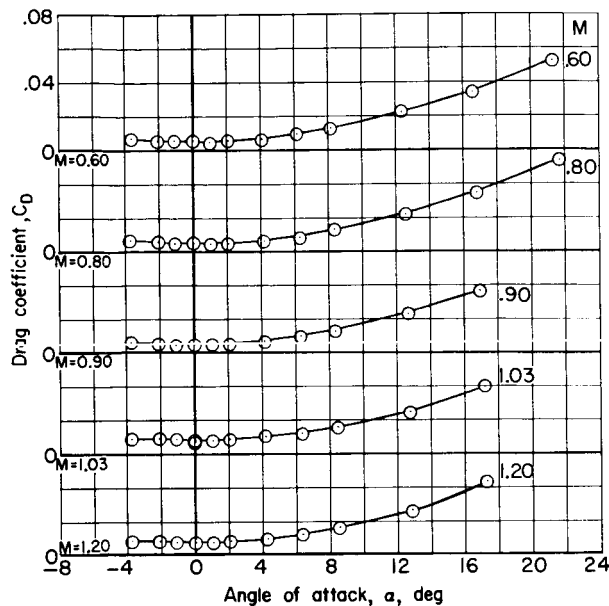
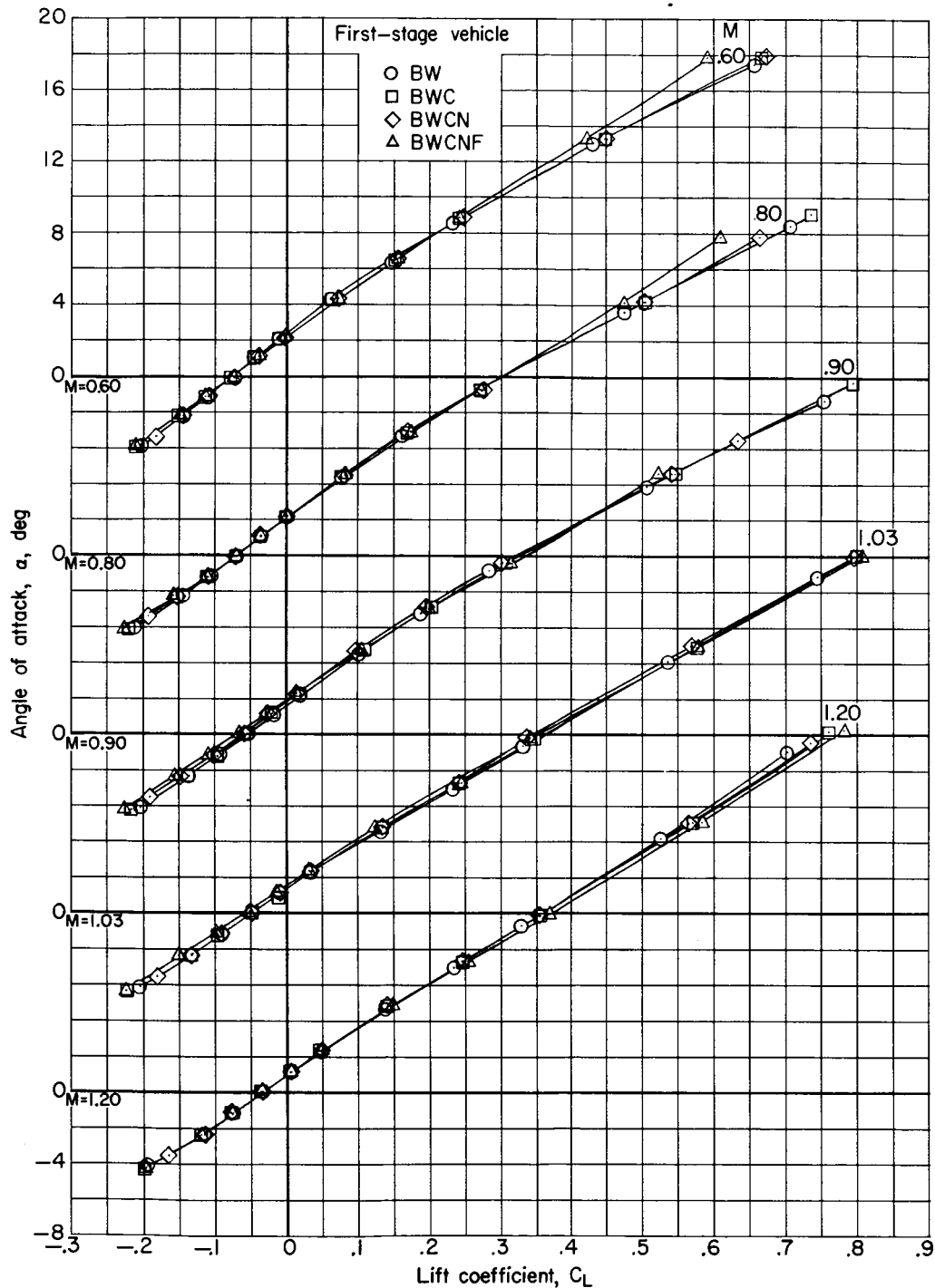
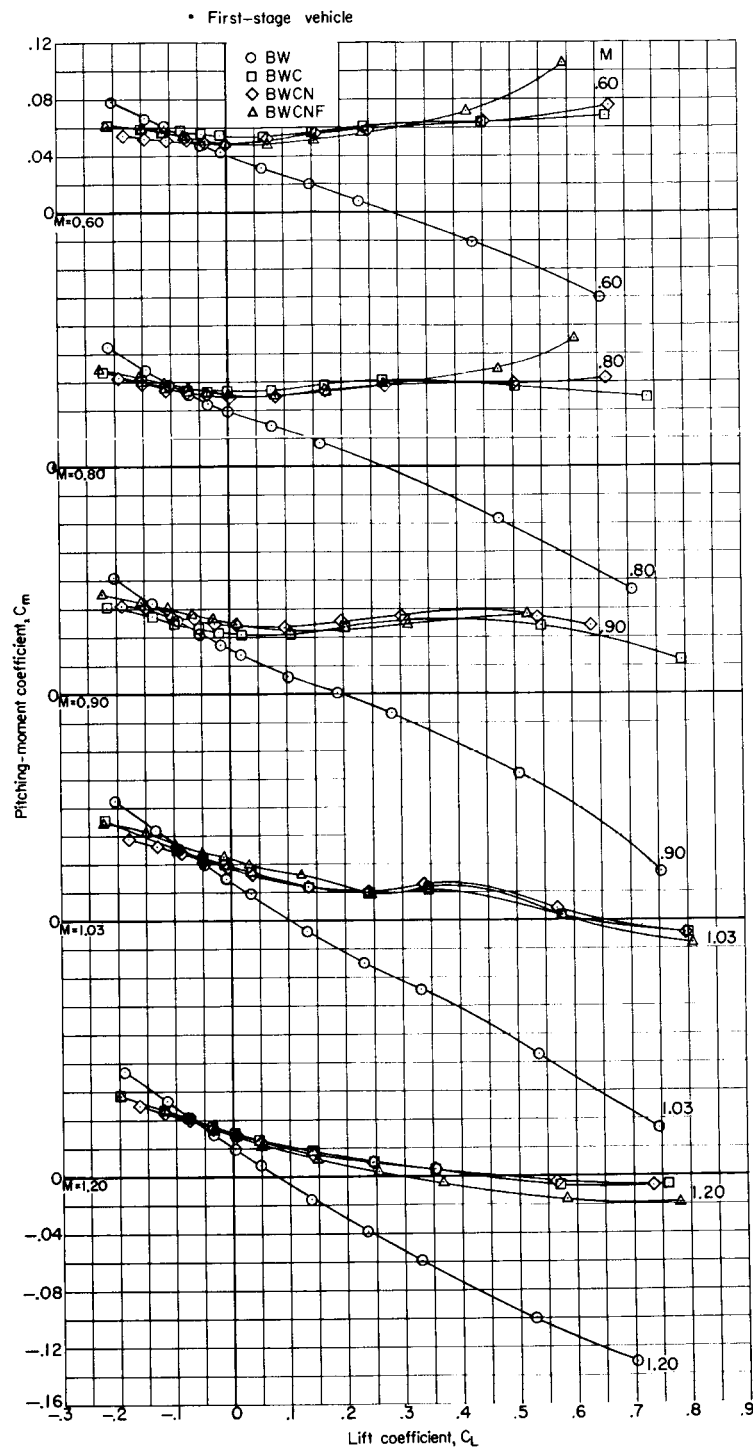


Figure 4.- Longitudinal aerodynamic characteristics for the first-stage fuselage.  $\beta = 0^\circ$ .



(a) Variation of angle of attack with lift coefficient.

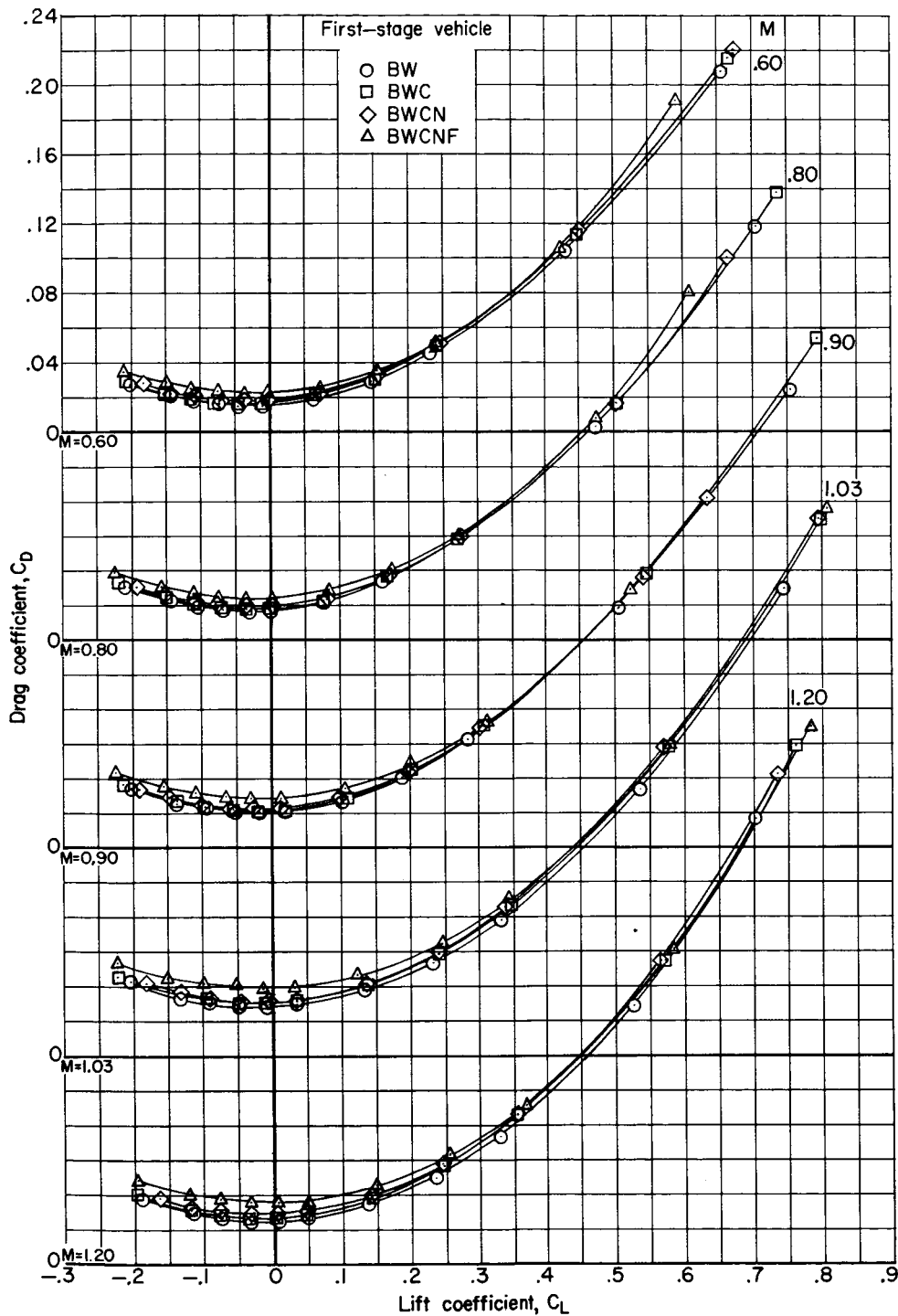
Figure 5.- Longitudinal aerodynamic characteristics for several first-stage configurations.  $\beta = 0^\circ$ .



(b) Variation of pitching-moment coefficient with lift coefficient.

Figure 5.- Continued.

~~UNCLASSIFIED~~

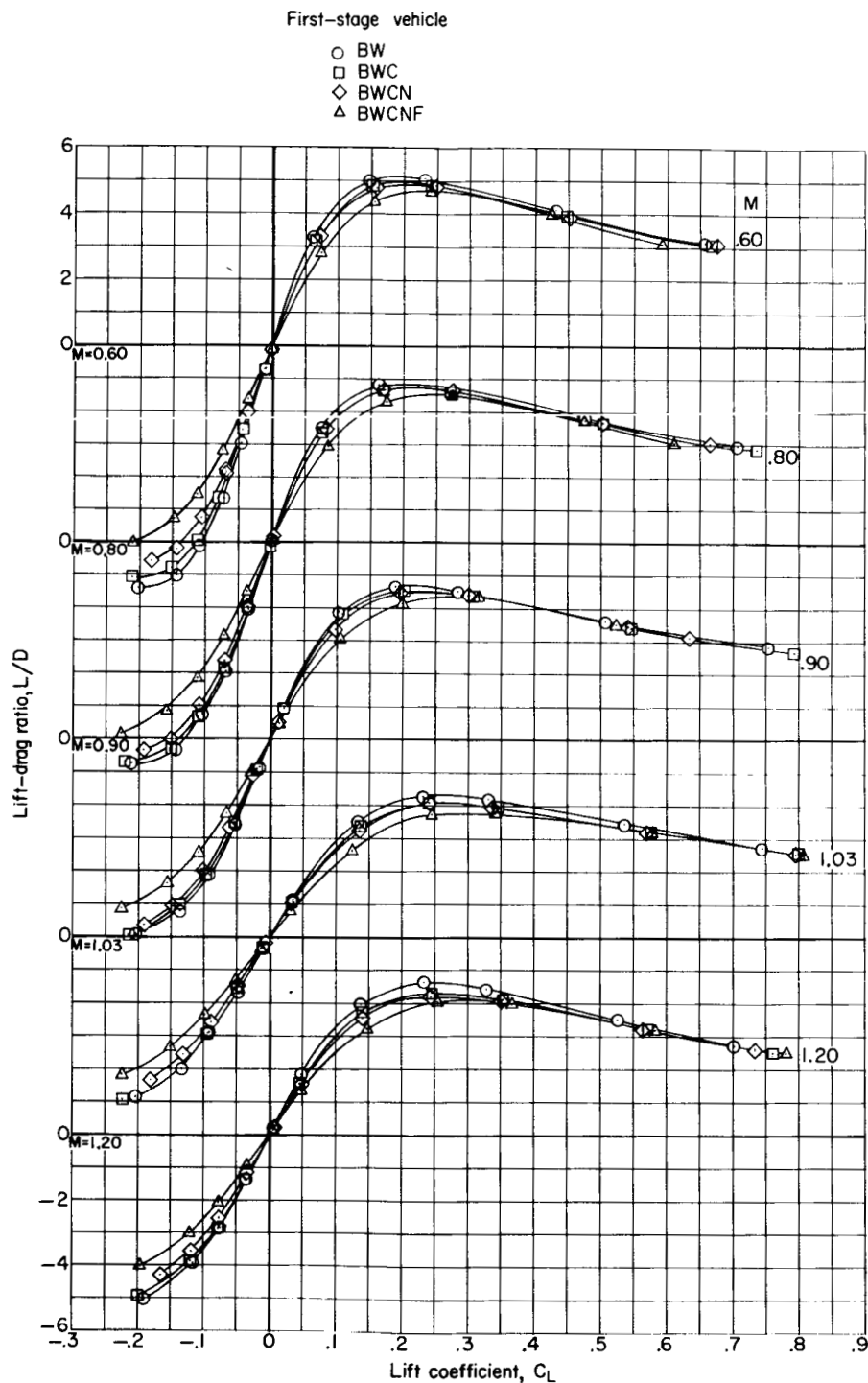


(c) Variation of drag coefficient with lift coefficient.

Figure 5.- Continued.

~~UNCLASSIFIED~~

UNCLASSIFIED

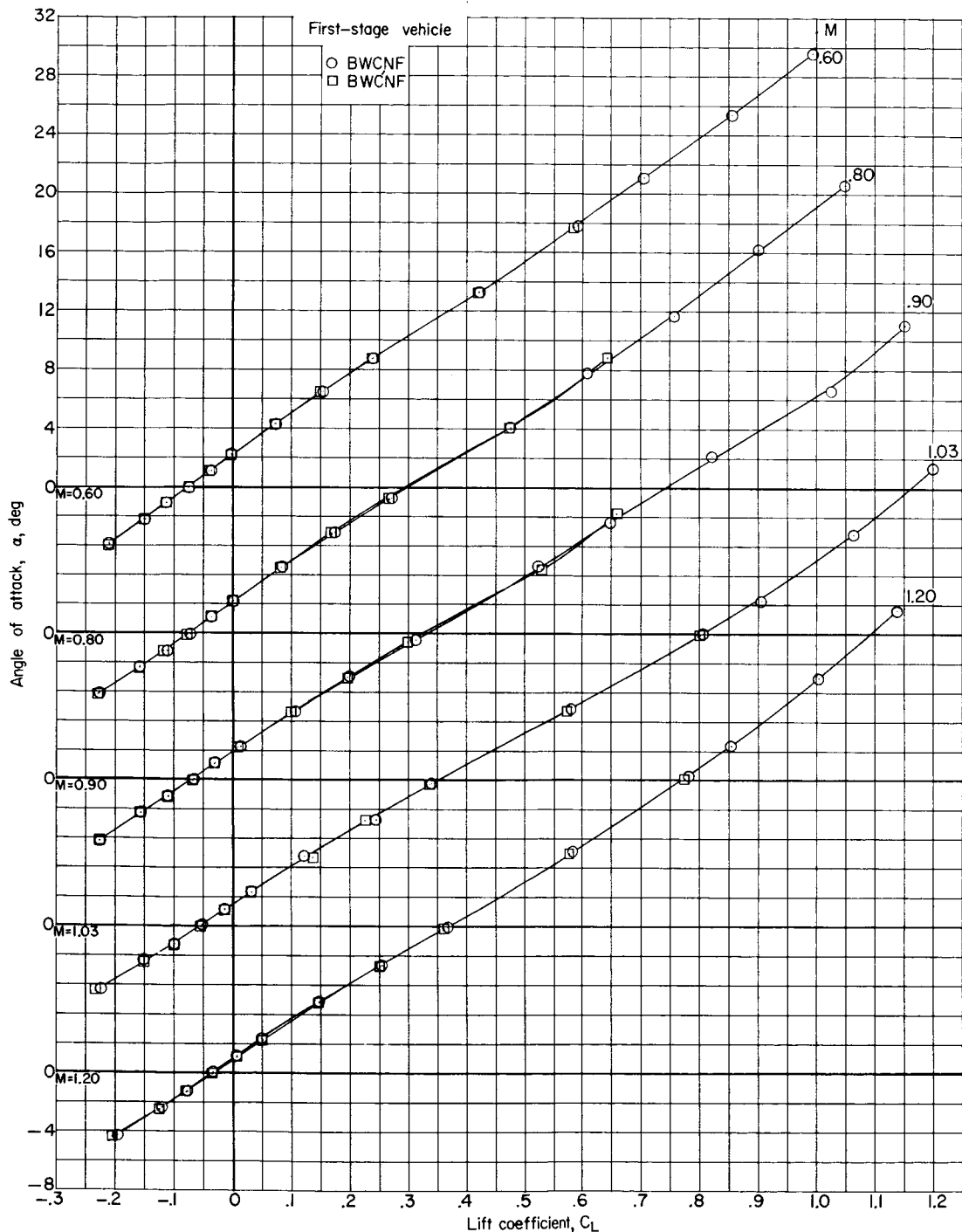


(d) Variation of lift-drag ratio with lift coefficient.

Figure 5.- Concluded.

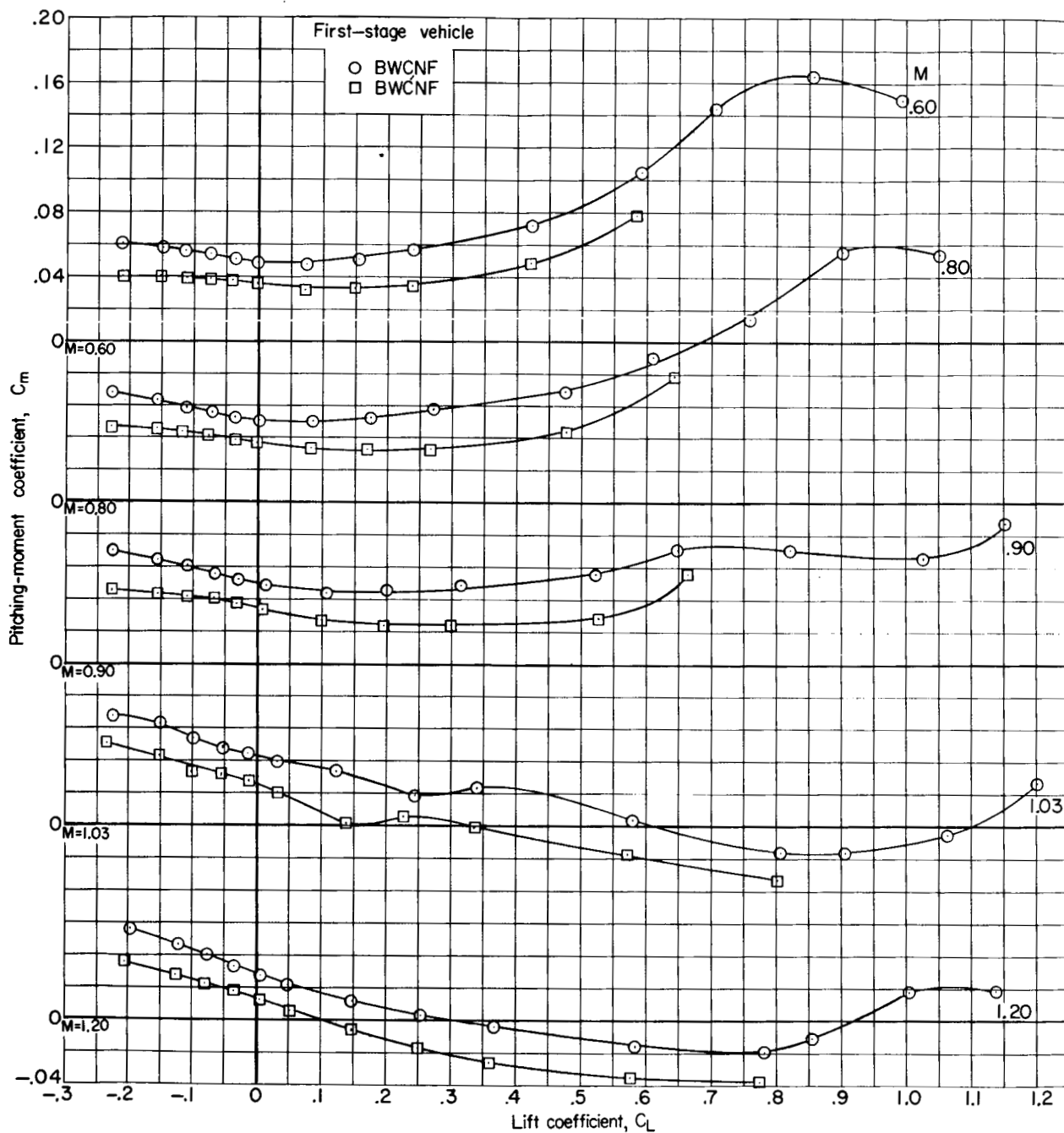
UNCLASSIFIED

UNCLASSIFIED



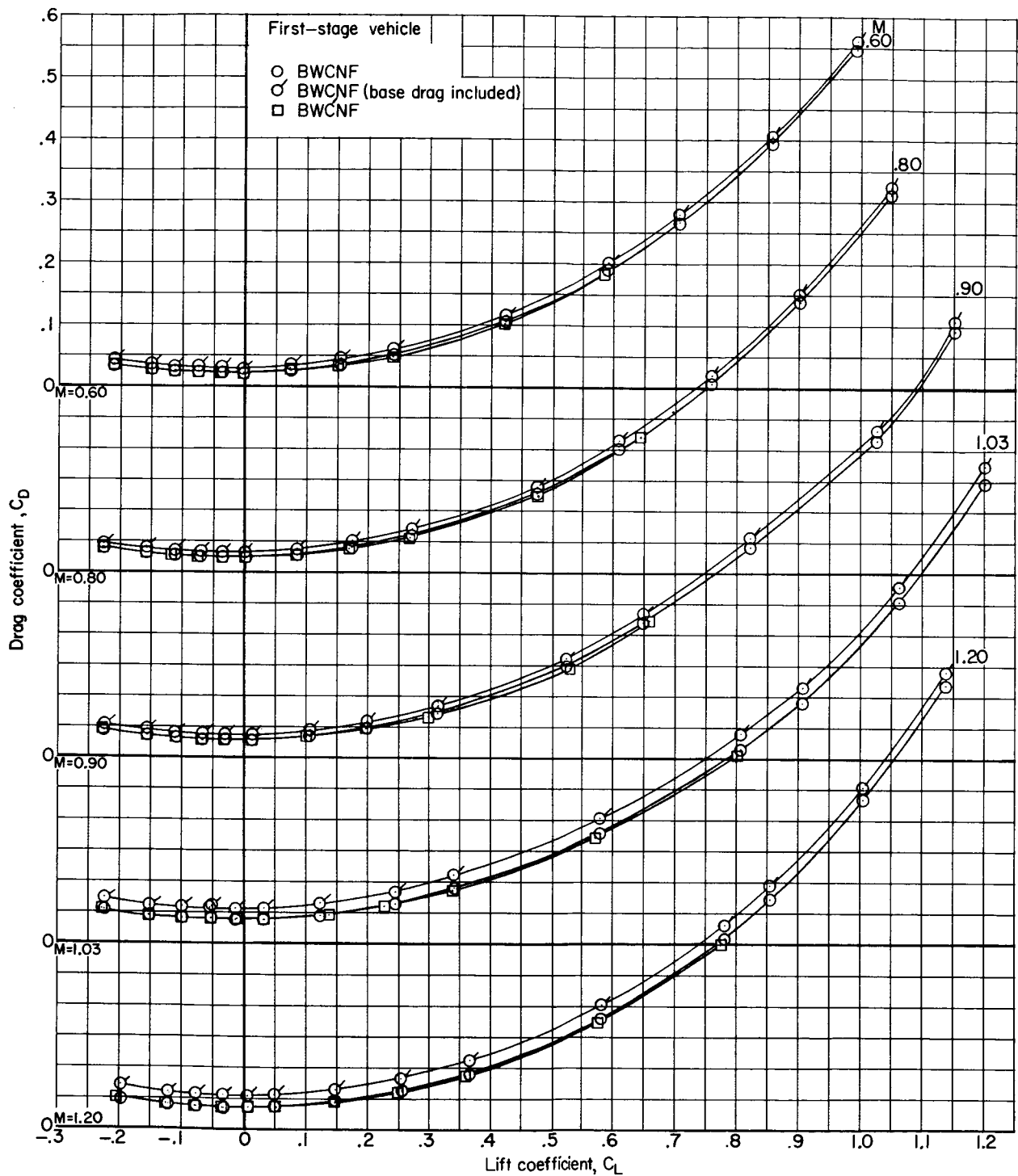
(a) Variation of angle of attack with lift coefficient.

Figure 6.- Longitudinal aerodynamic characteristics for the first-stage reusable booster with the canard at  $0^\circ$  and  $-5^\circ$  deflection.  $\beta = 0^\circ$ .



(b) Variation of pitching-moment coefficient with lift coefficient.

Figure 6.- Continued.

~~CONFIDENTIAL~~

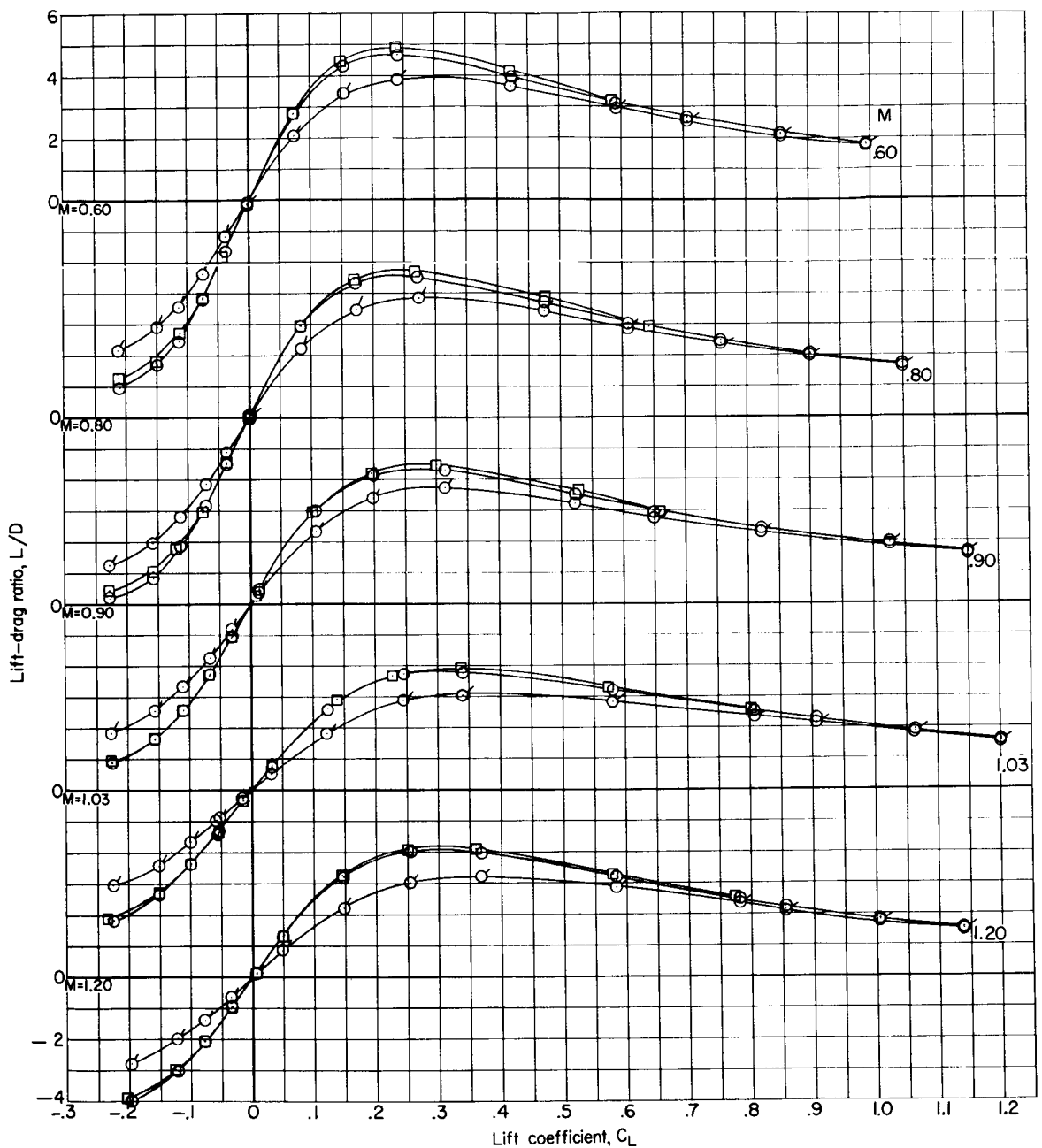
(c) Variation of drag coefficient with lift coefficient.

Figure 6.- Continued.

~~CONFIDENTIAL~~

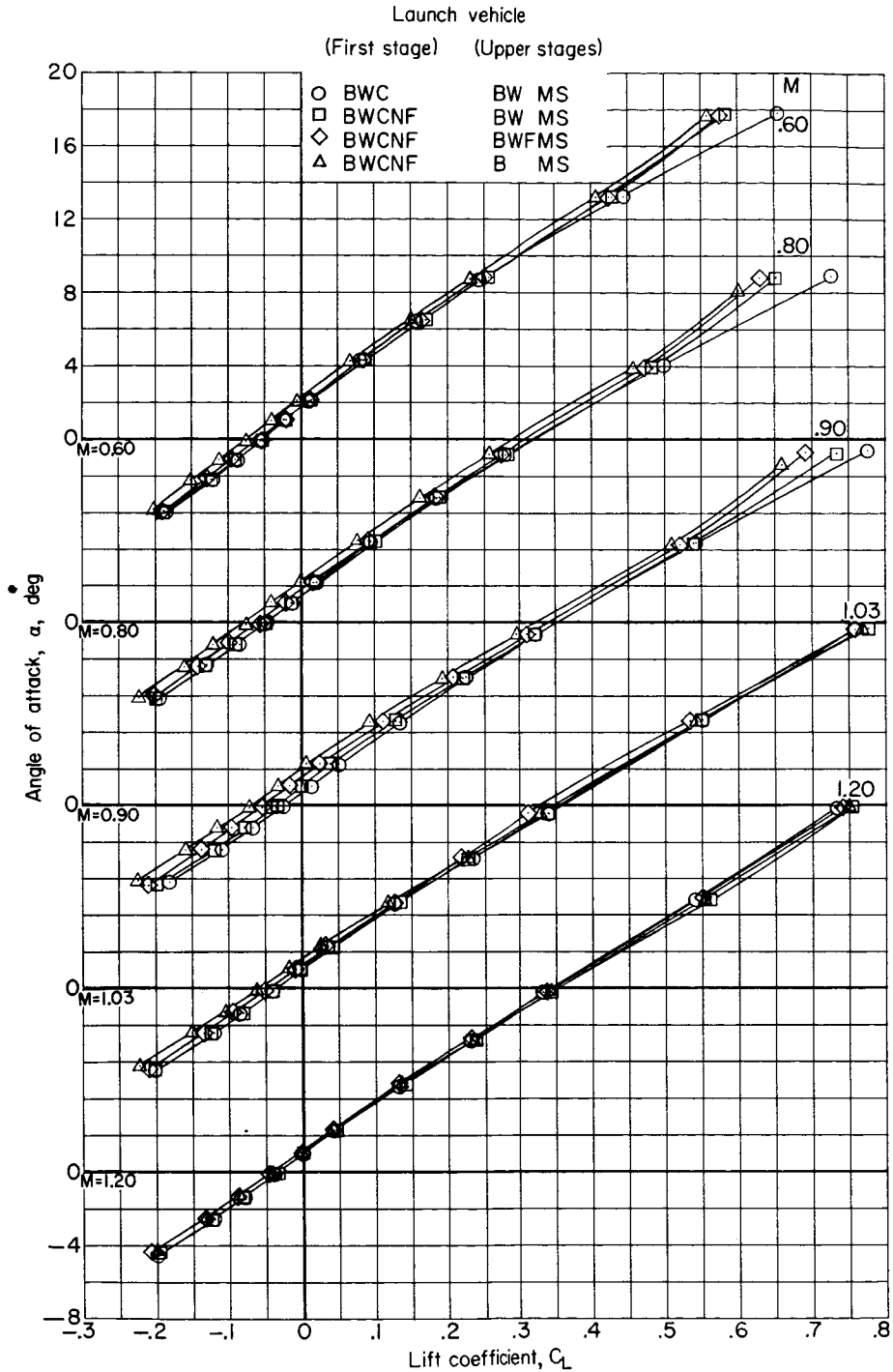
First-stage vehicle

- BWCNF  
 ○ BWCNF (base drag included)  
 □ BWCNF



(d) Variation of lift-drag ratio with lift coefficient.

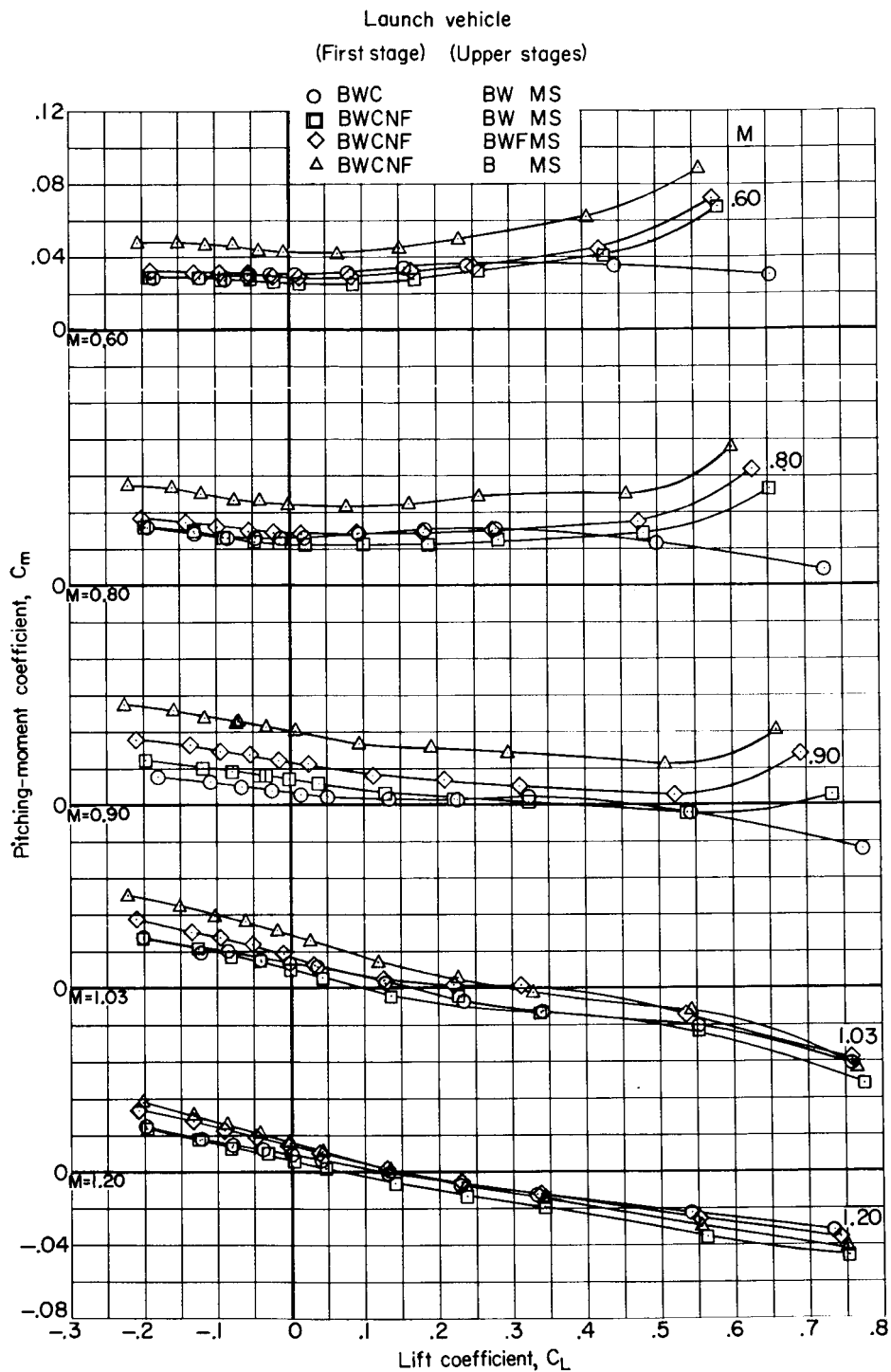
Figure 6.- Concluded.

~~CONFIDENTIAL~~

(a) Variation of angle of attack with lift coefficient.

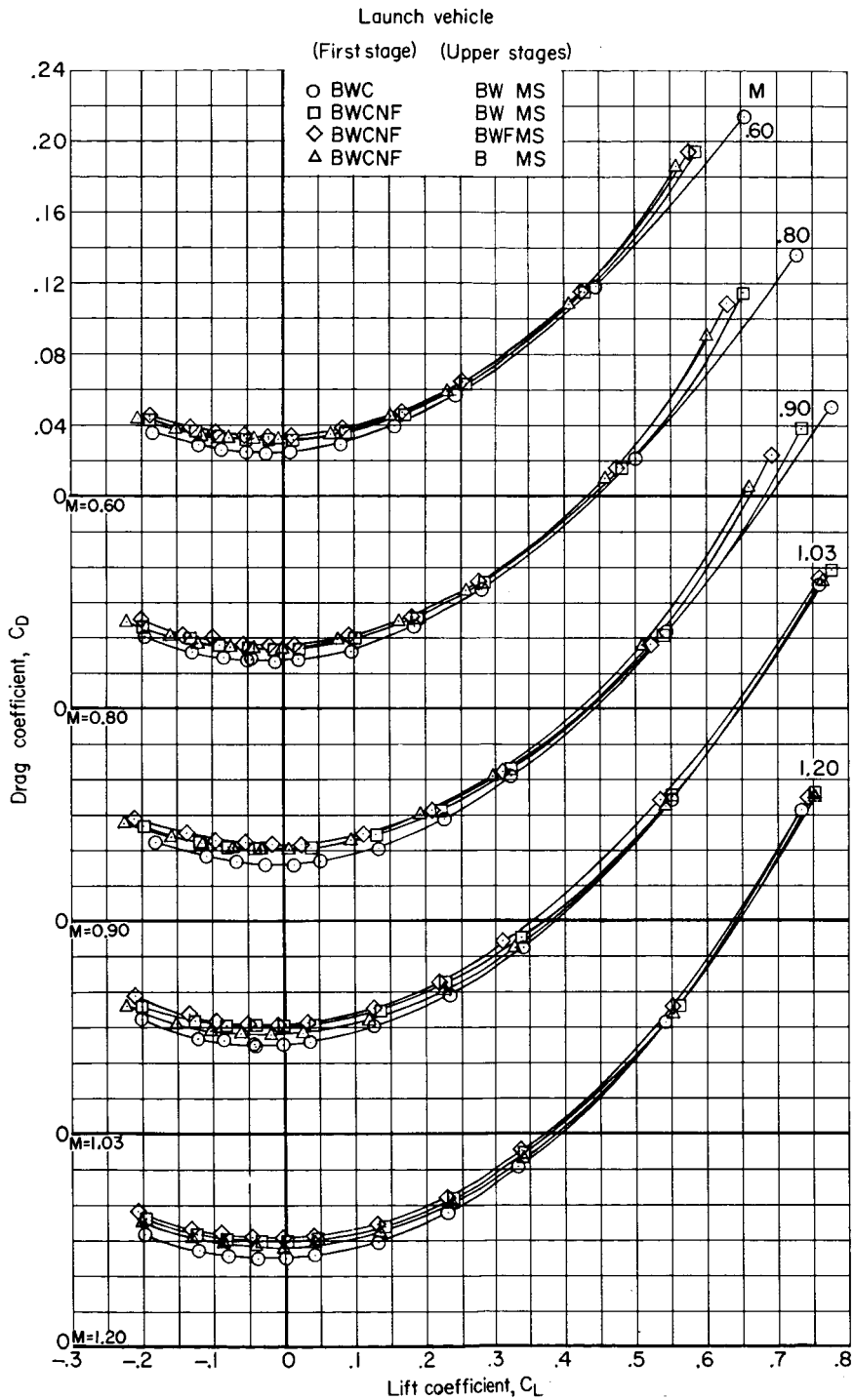
Figure 7.- Longitudinal aerodynamic characteristics for several launch configurations with the effects of the second-stage wing and the first- and second-stage vertical fins.  $\beta = 0^\circ$ .

~~CONFIDENTIAL~~



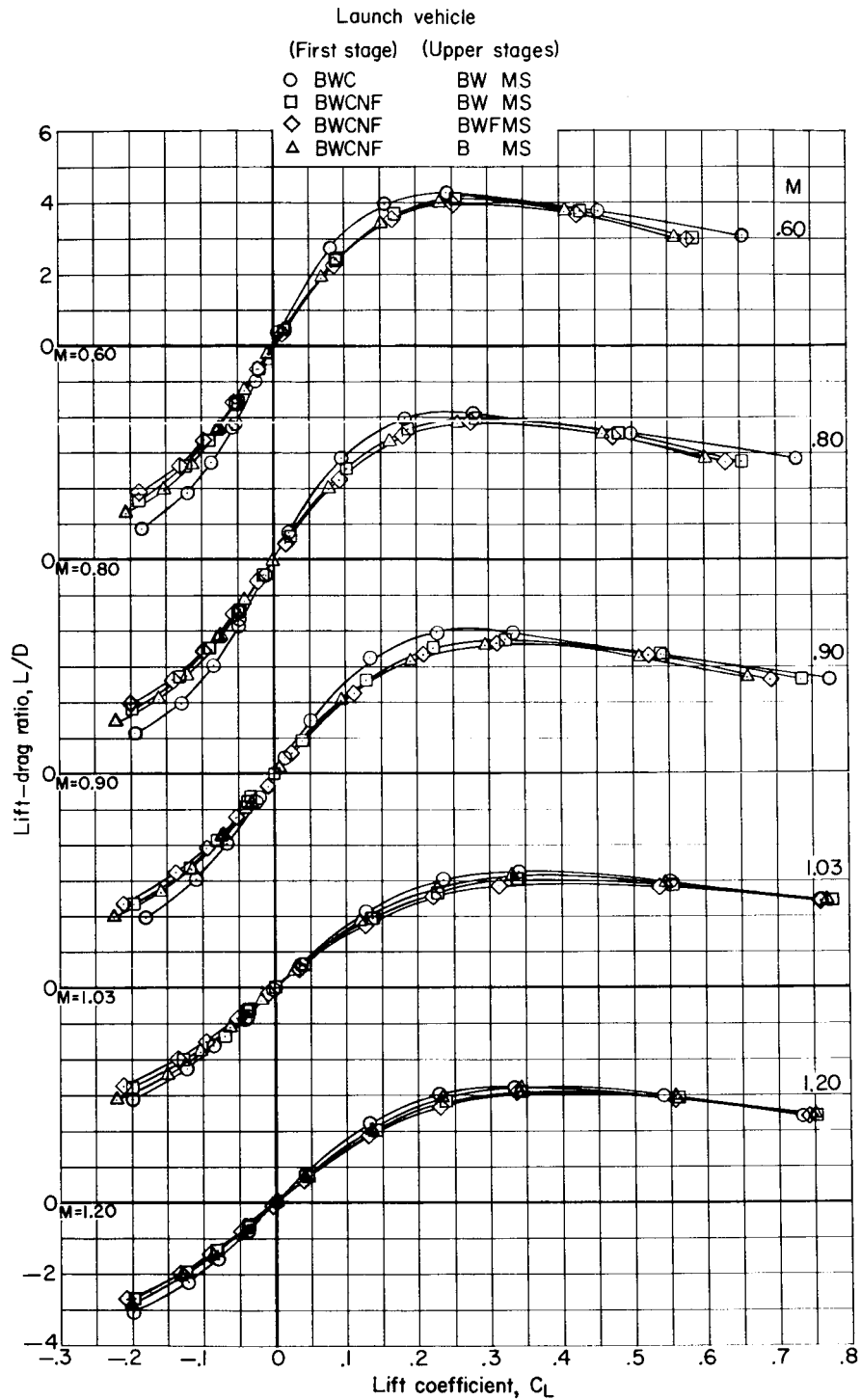
(b) Variation of pitching-moment coefficient with lift coefficient.

Figure 7.- Continued.



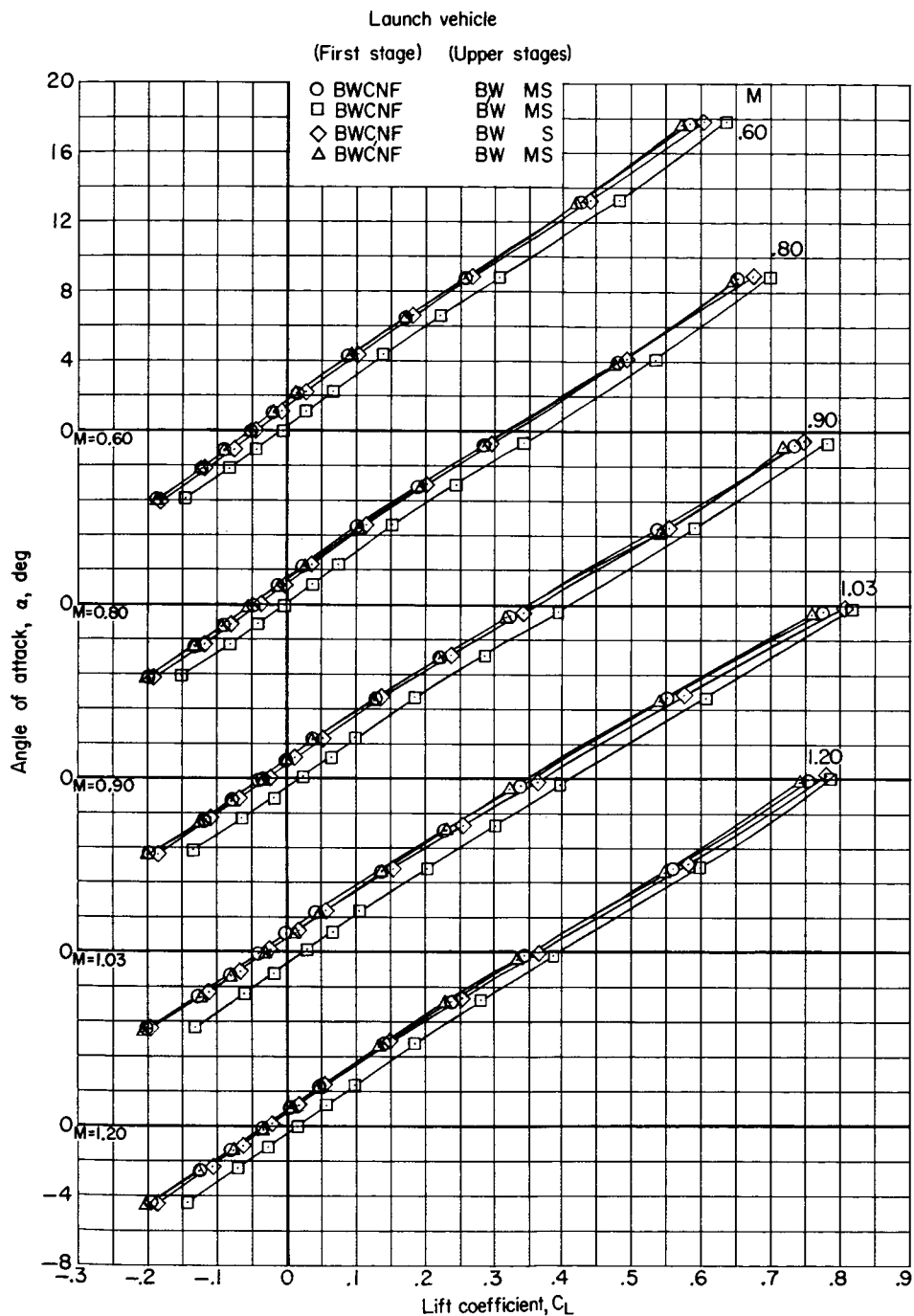
(c) Variation of drag coefficient with lift coefficient.

Figure 7.- Continued.



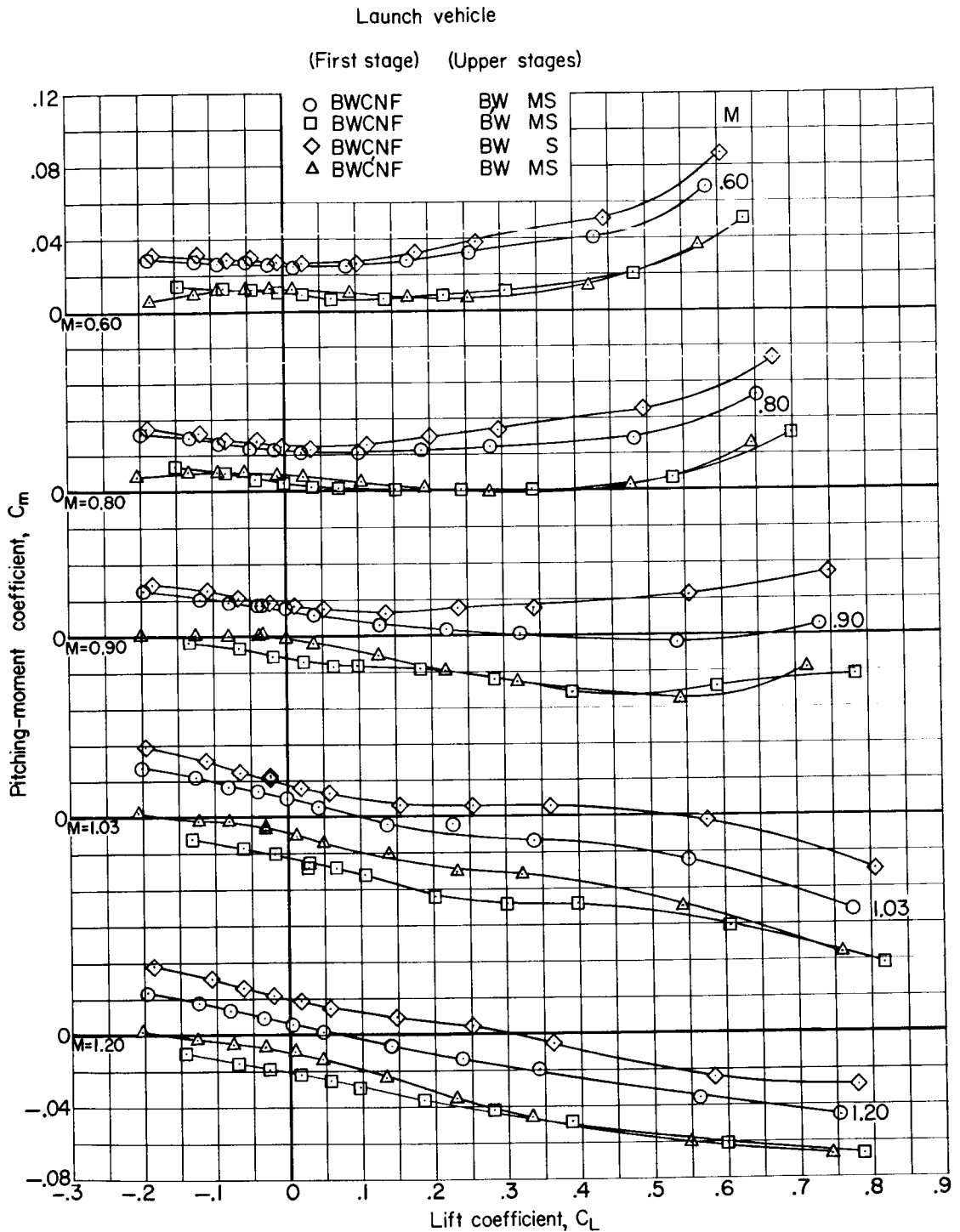
(d) Variation of lift-drag ratio with lift coefficient.

Figure 7.- Concluded.



(a) Variation of angle of attack with lift coefficient.

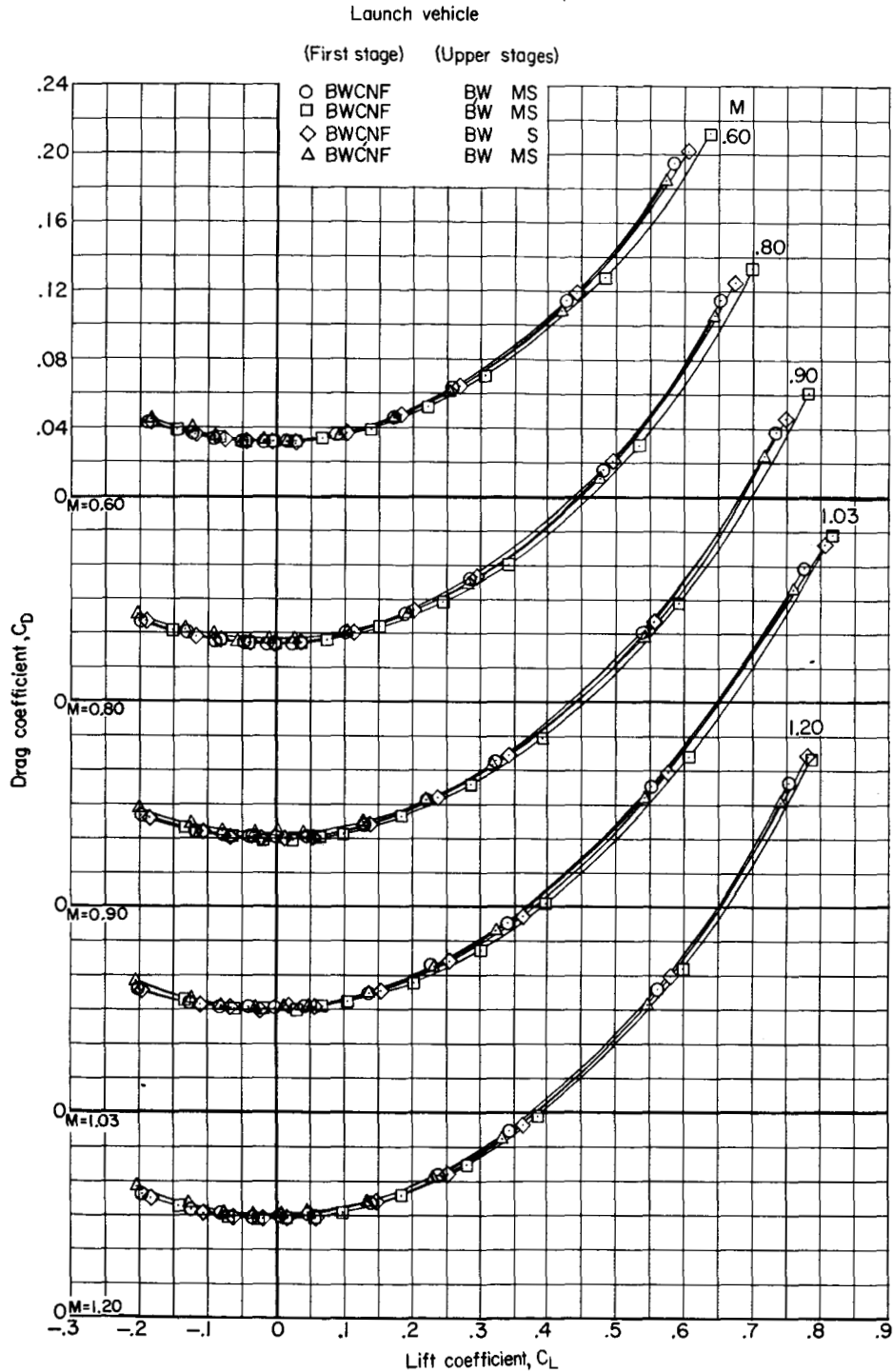
Figure 8.- Longitudinal aerodynamic characteristics for several launch configurations with the effects of a second-stage afterbody fairing, the maneuver stage, and a canard deflection of  $-5^\circ$ .  $\beta = 0^\circ$ .



(b) Variation of pitching-moment coefficient with lift coefficient.

Figure 8.- Continued.

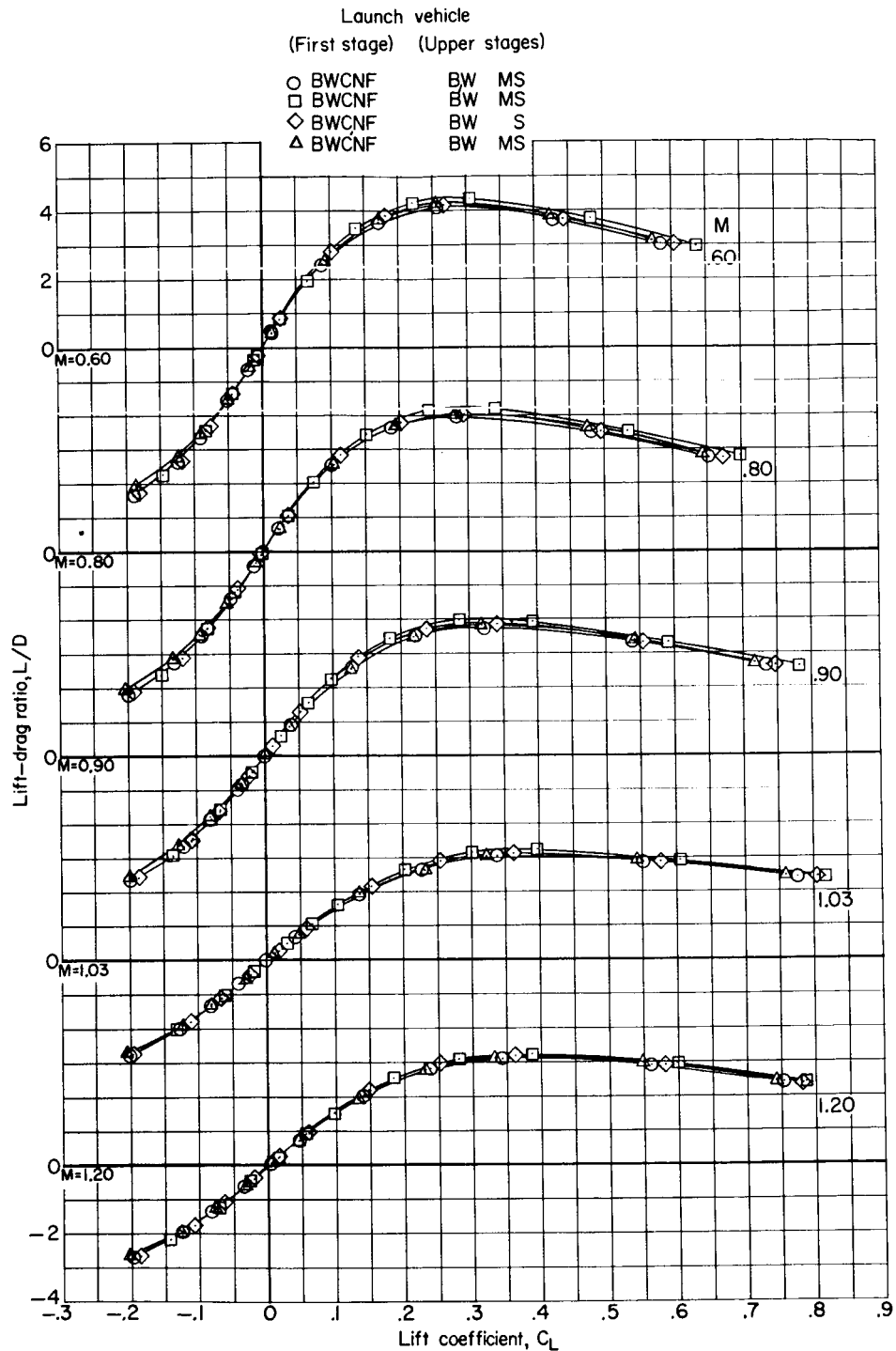
UNCLASSIFIED



(c) Variation of drag coefficient with lift coefficient.

Figure 8.- Continued.

UNCLASSIFIED



(d) Variation of lift-drag ratio with lift coefficient.

Figure 8.- Concluded.

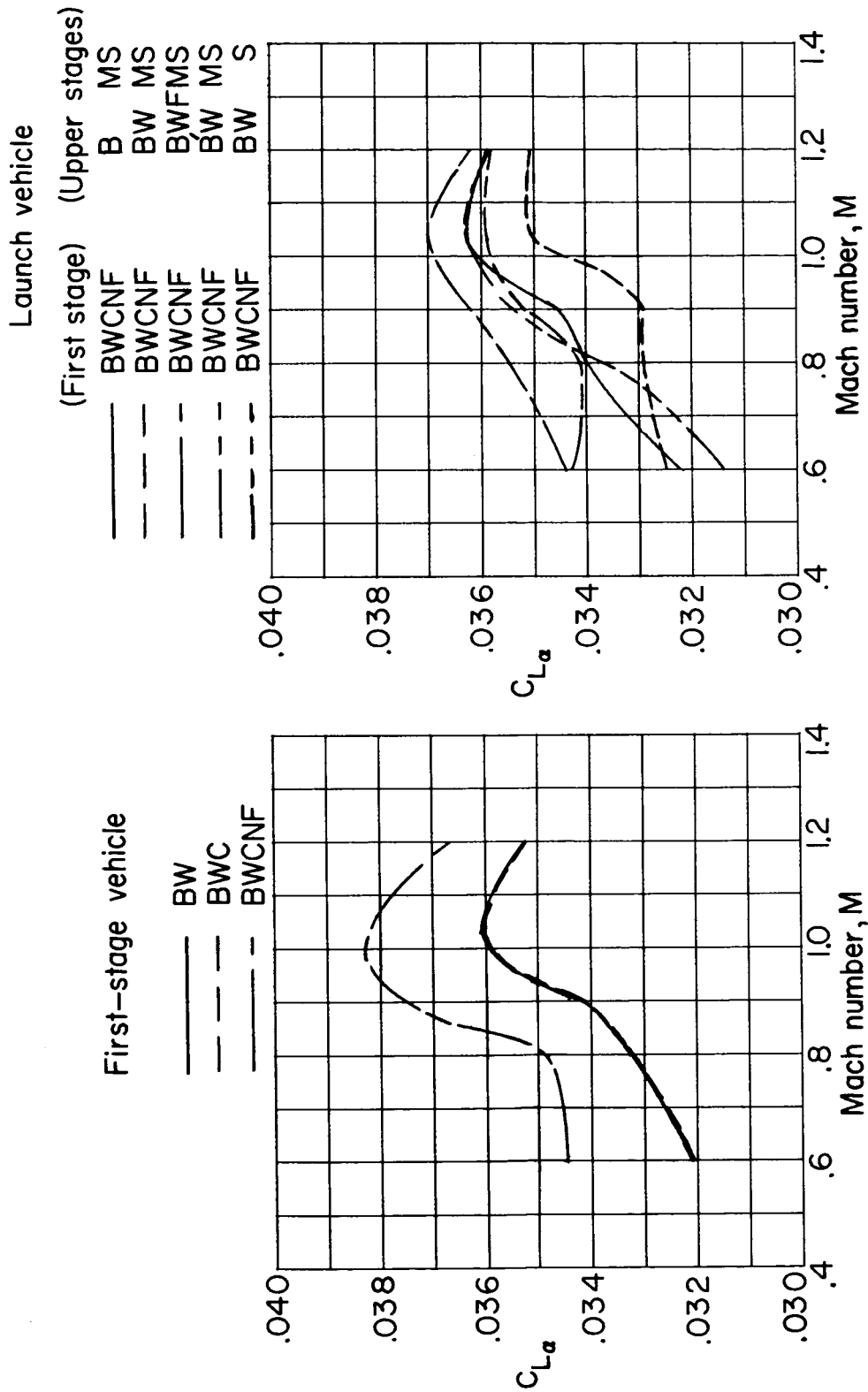


Figure 9.- Variation with Mach number of the lift-curve slopes for several first-stage and launch configurations.  $\beta = 0^\circ$ .



Figure 10.- Variation with Mach number of the longitudinal-stability parameters for several first-stage and launch configurations and the canard effectiveness for a first-stage and a launch configuration.  $\beta = 0^\circ$ .

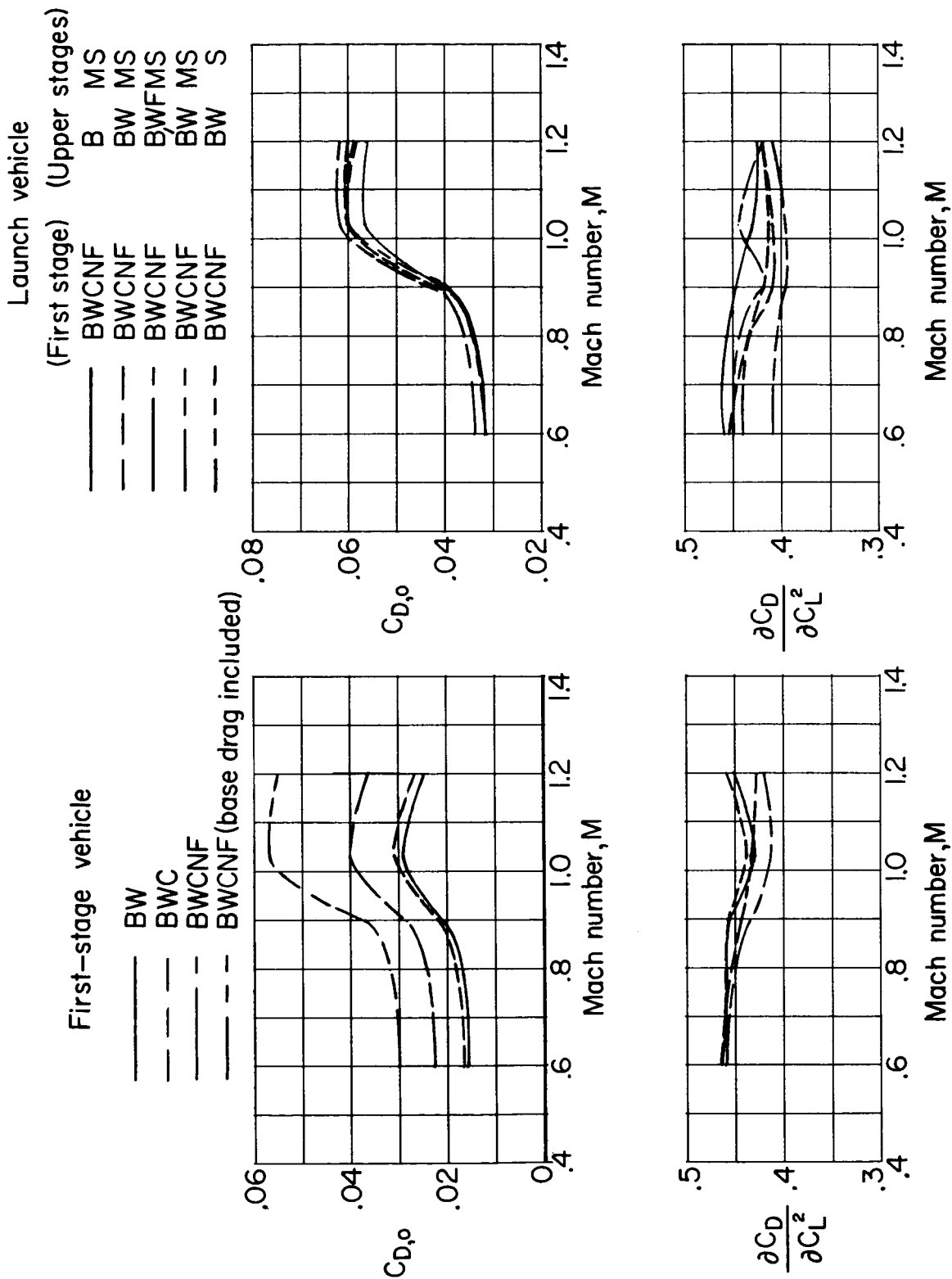


Figure 11.- Variation with Mach number of the drag-at-zero-lift and the drag-due-to-lift parameters for several first-stage and launch configurations.  $\beta = 0^\circ$ .

UNCLASSIFIED

CONFIDENTIAL

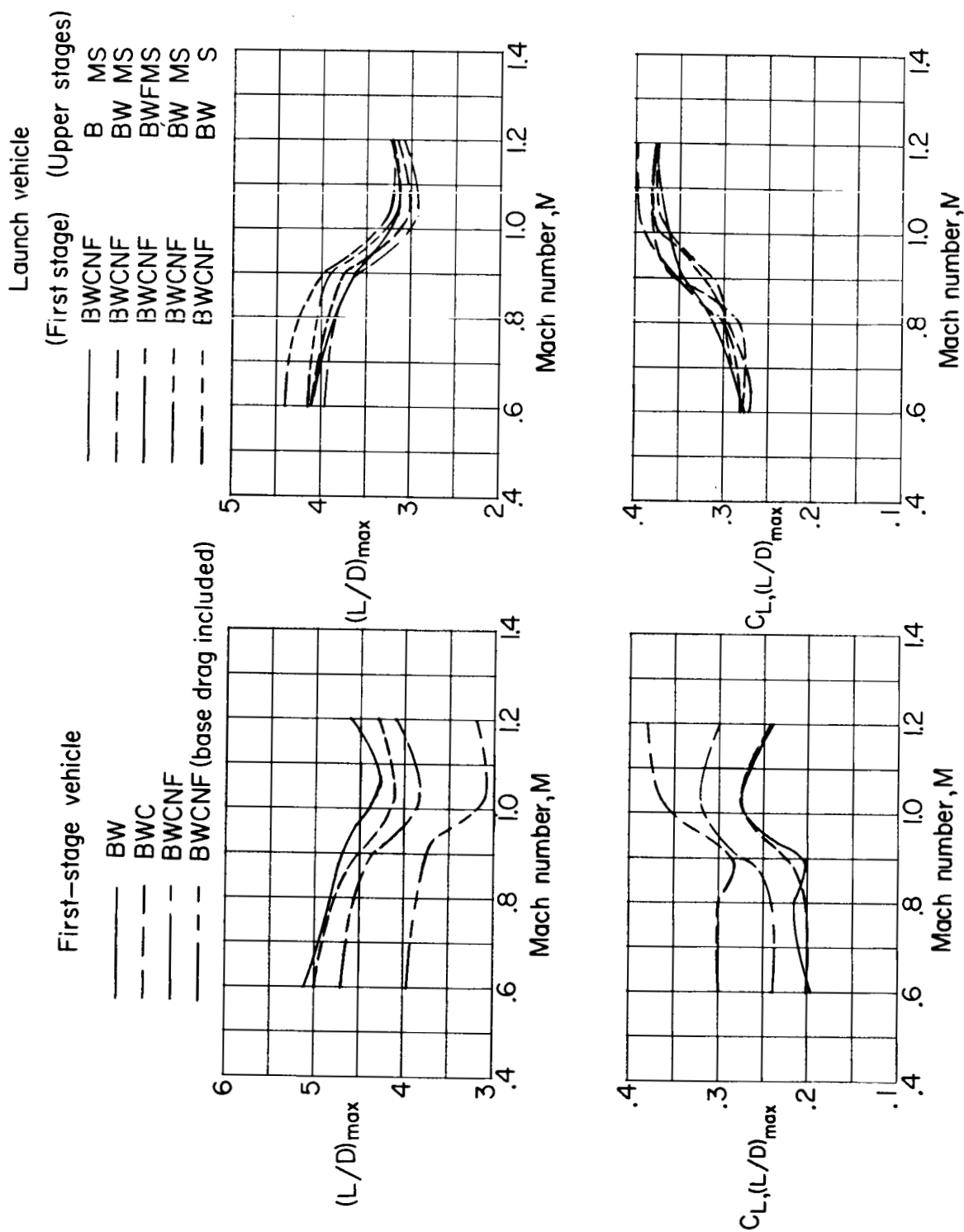
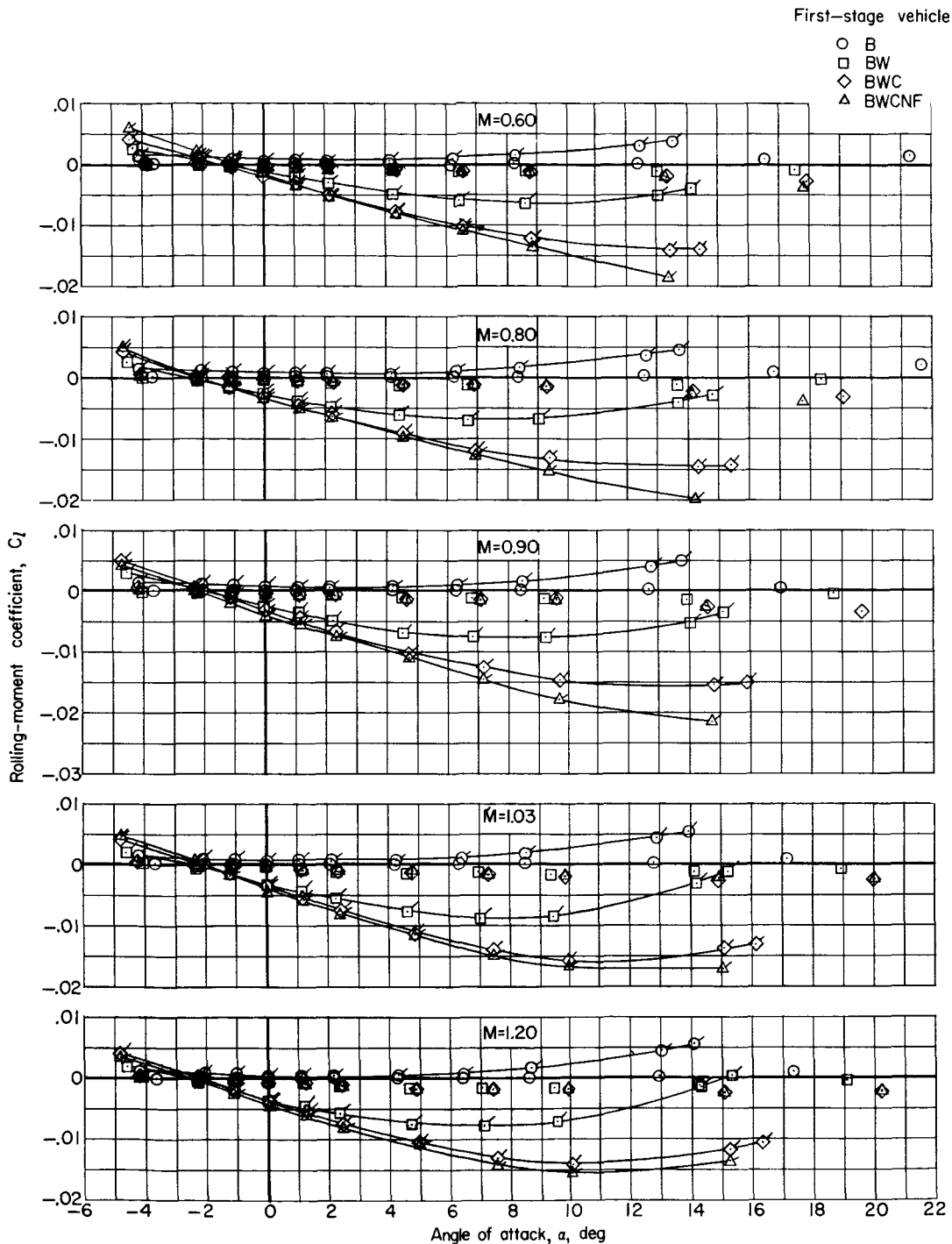


Figure 12.- Variation with Mach number of the maximum lift-drag ratio and the lift coefficient at which maximum lift-drag ratio occurs for several first-stage and launch configurations.  $\beta = 0^\circ$ .

UNCLASSIFIED

# UNCLASSIFIED

~~CONFIDENTIAL~~

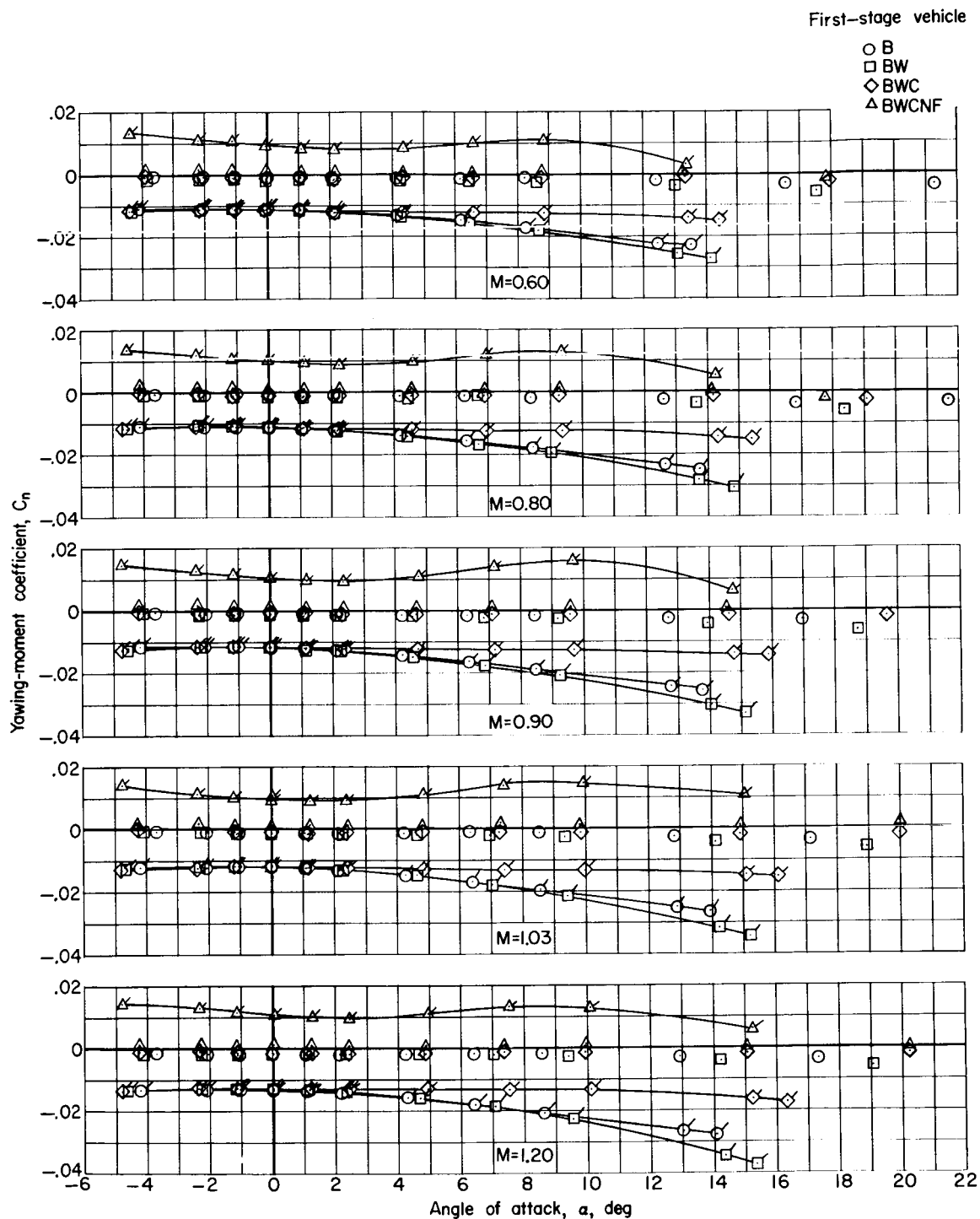


(a) Variation of rolling-moment coefficient with angle of attack.

Figure 13.- Lateral aerodynamic characteristics for several first-stage configurations.  $\beta = 0^\circ$  and  $5^\circ$ . (Flagged symbols refer to  $\beta = 5^\circ$ .)

~~CONFIDENTIAL~~

# UNCLASSIFIED

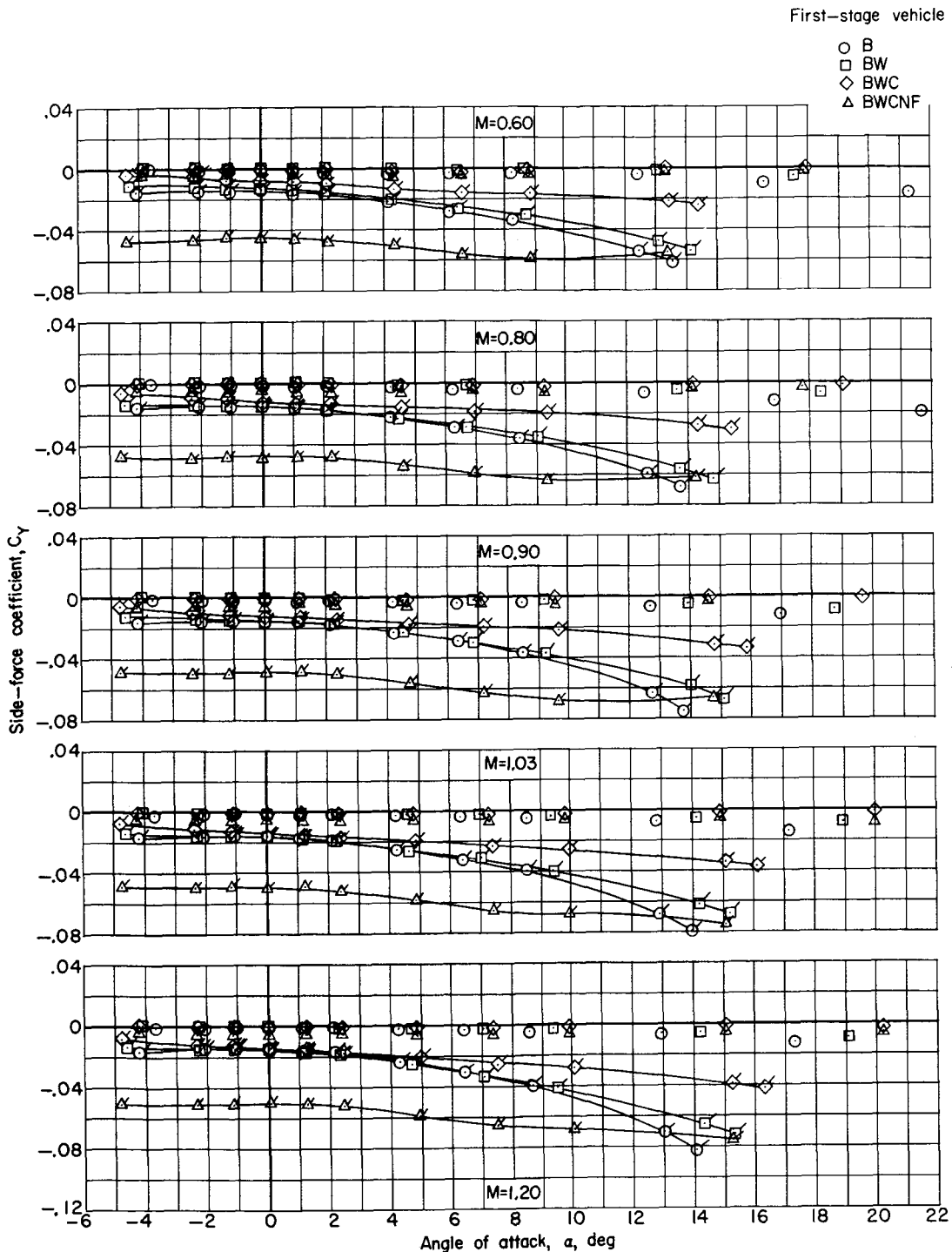


(b) Variation of yawing-moment coefficient with angle of attack.

Figure 13.- Continued.

UNCLASSIFIED

~~CONFIDENTIAL~~

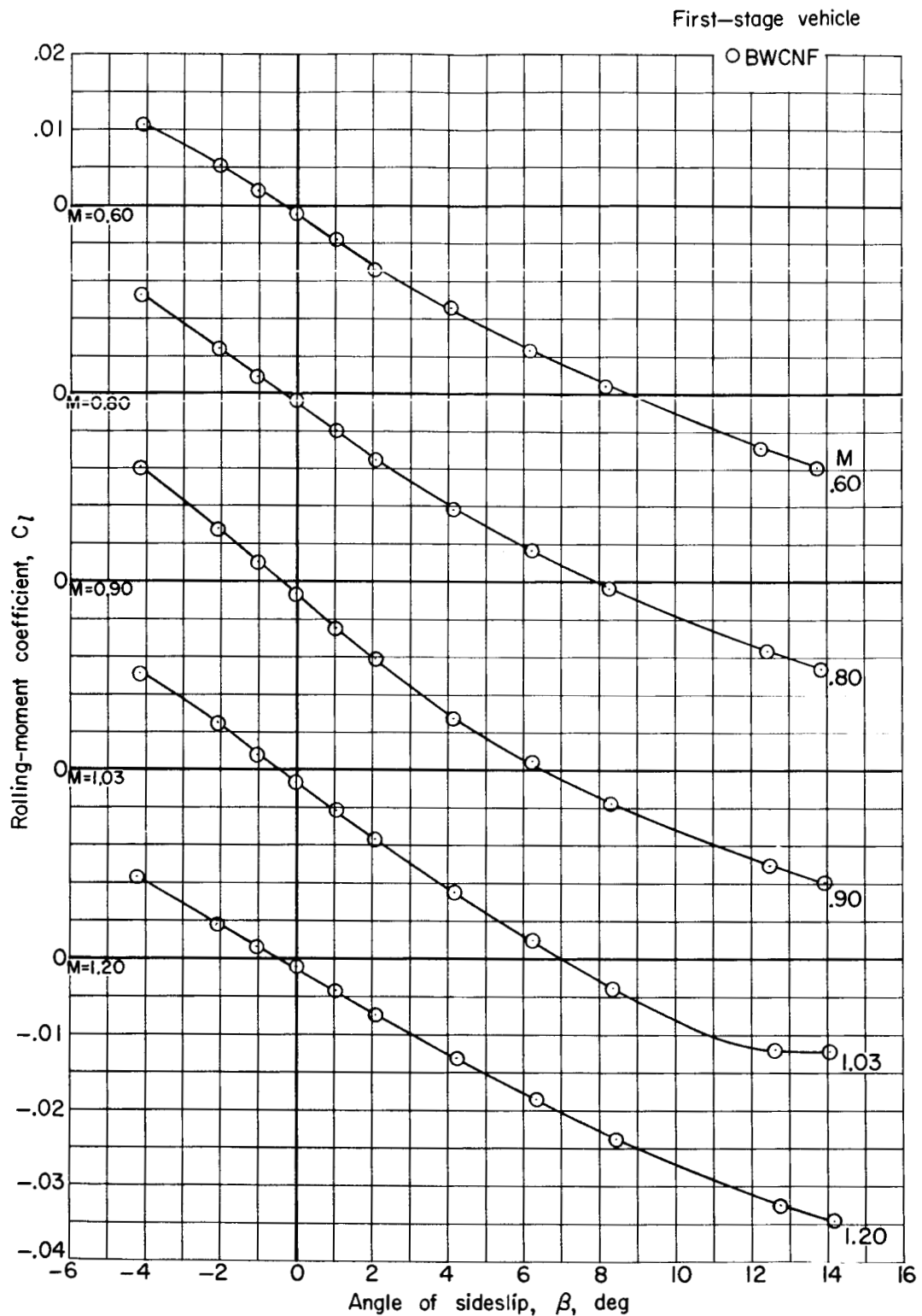


(c) Variation of side-force coefficient with angle of attack.

Figure 13.- Concluded.

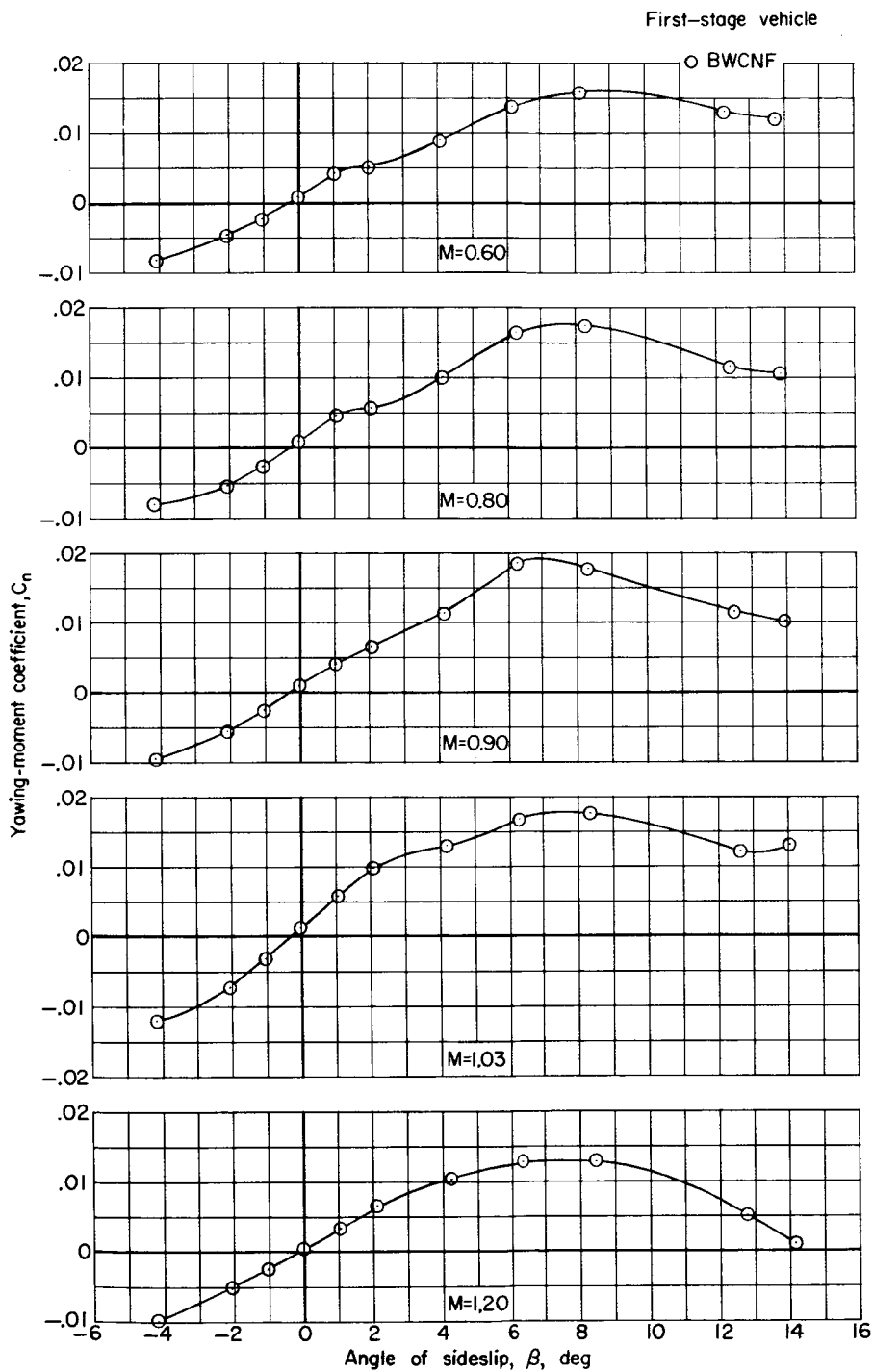
~~CONFIDENTIAL~~

UNCLASSIFIED



(a) Variation of rolling-moment coefficient with angle of sideslip.

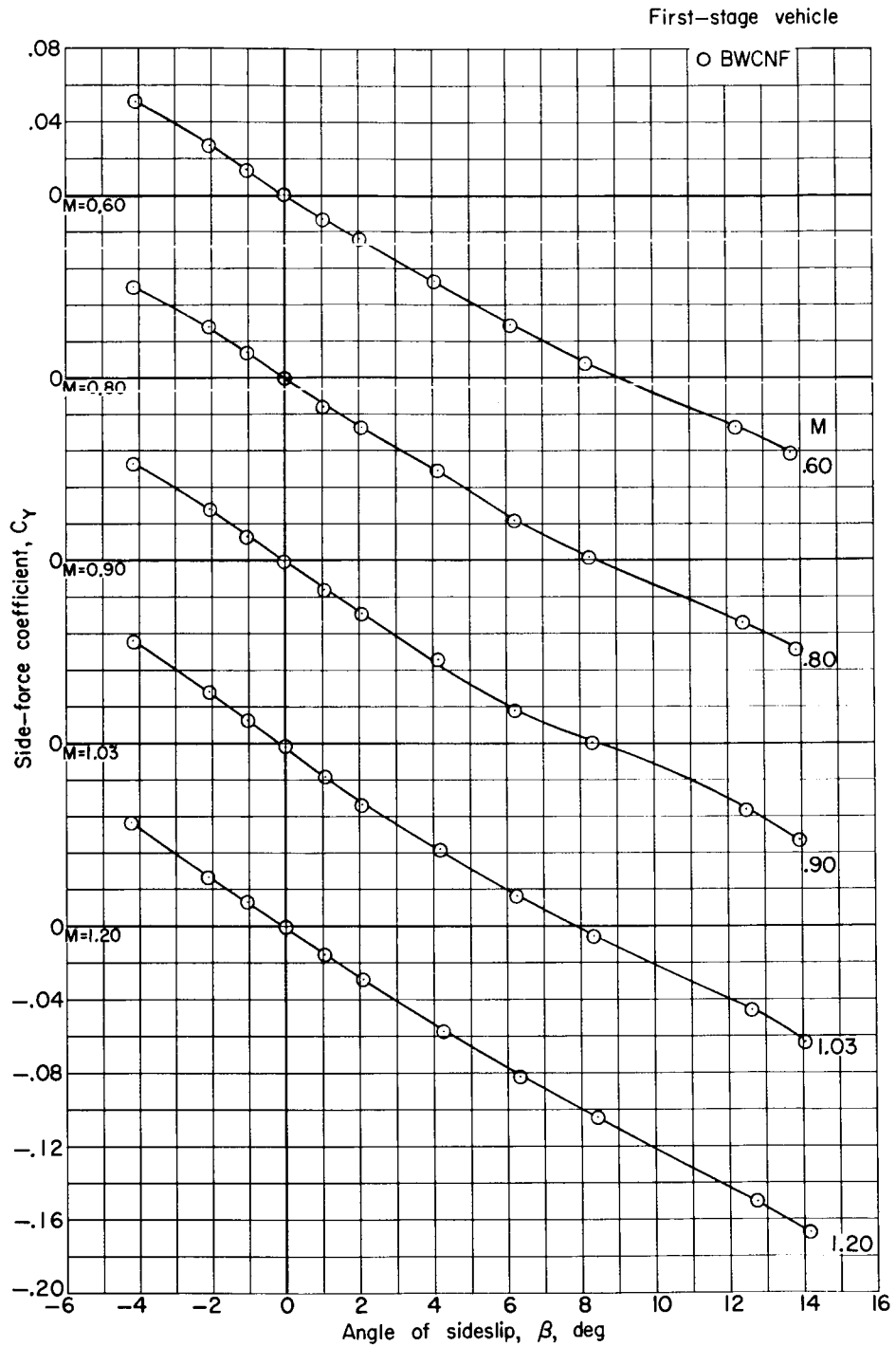
Figure 14.- Lateral aerodynamic characteristics for the first-stage reusable booster.  $\alpha = 10^\circ$ .



(b) Variation of yawing-moment coefficient with angle of sideslip.

Figure 14.- Continued.

UNCLASSIFIED



(c) Variation of side-force coefficient with angle of sideslip.

Figure 14.- Concluded.

UNCLASSIFIED

# UNCLASSIFIED

~~CONFIDENTIAL~~

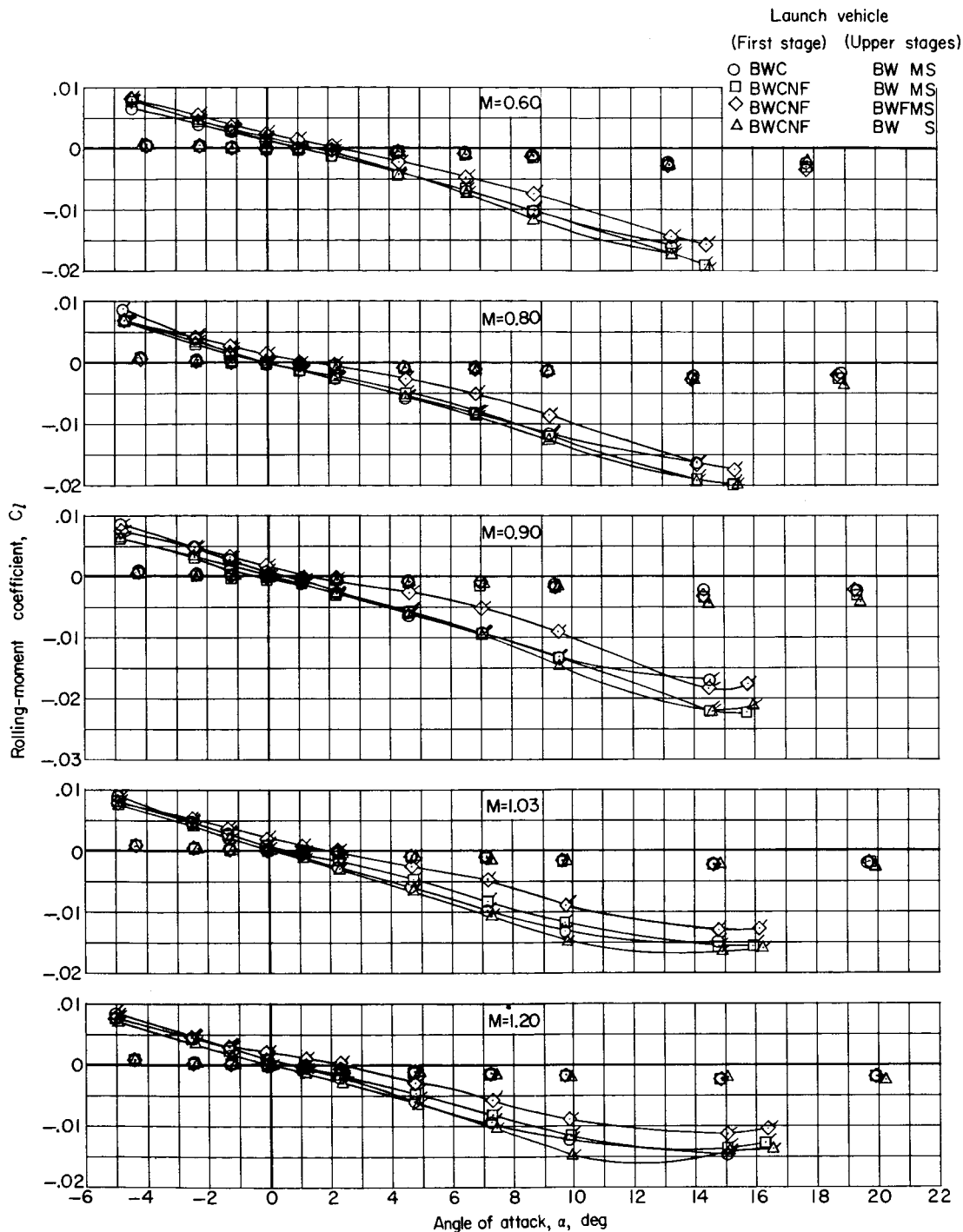
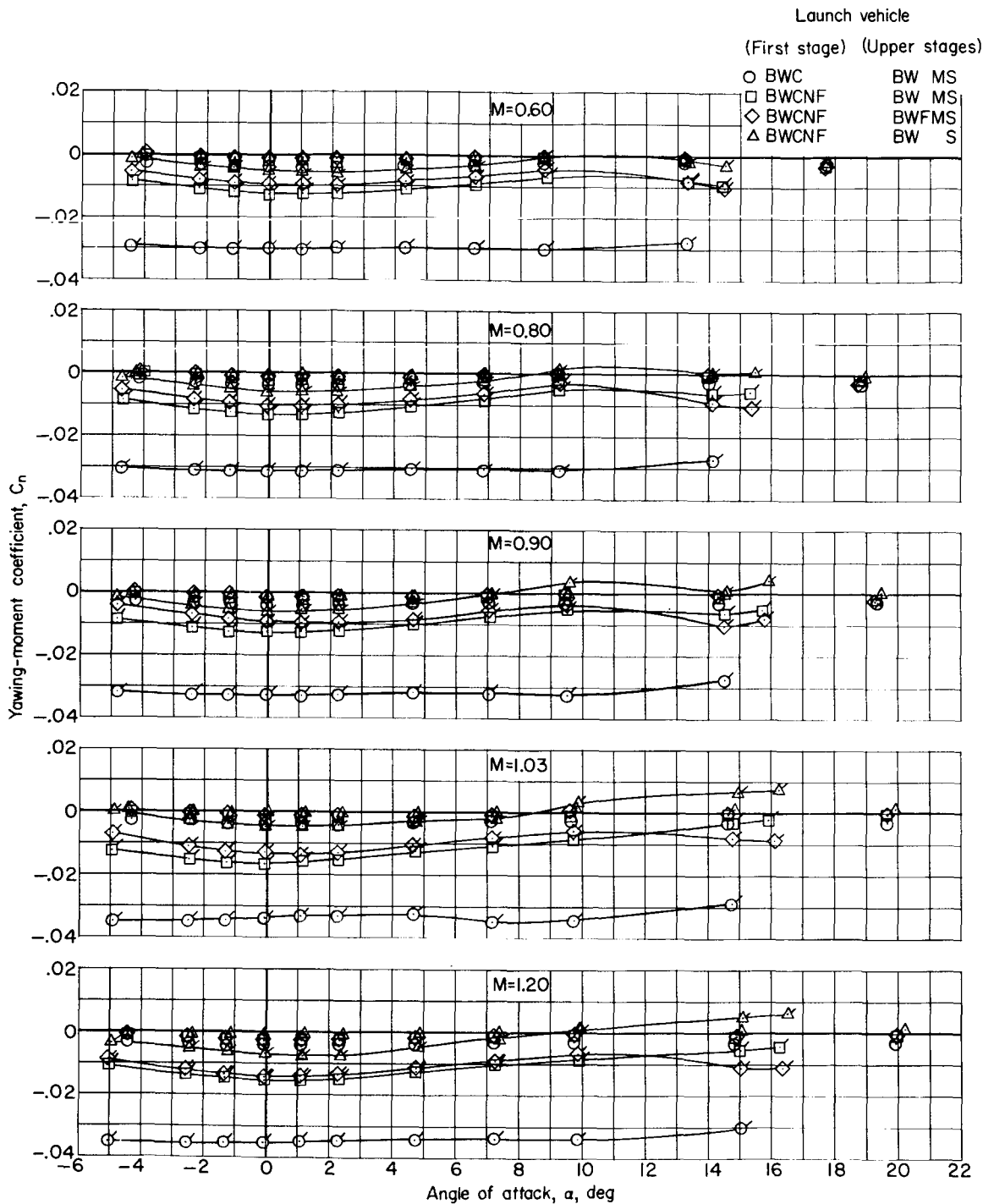


Figure 15.- Lateral aerodynamic characteristics for several launch configurations.  $\beta = 0^\circ$  and  $5^\circ$ .  
(Flagged symbols refer to  $\beta = 5^\circ$ .)

~~CONFIDENTIAL~~

# UNCLASSIFIED

# UNCLASSIFIED

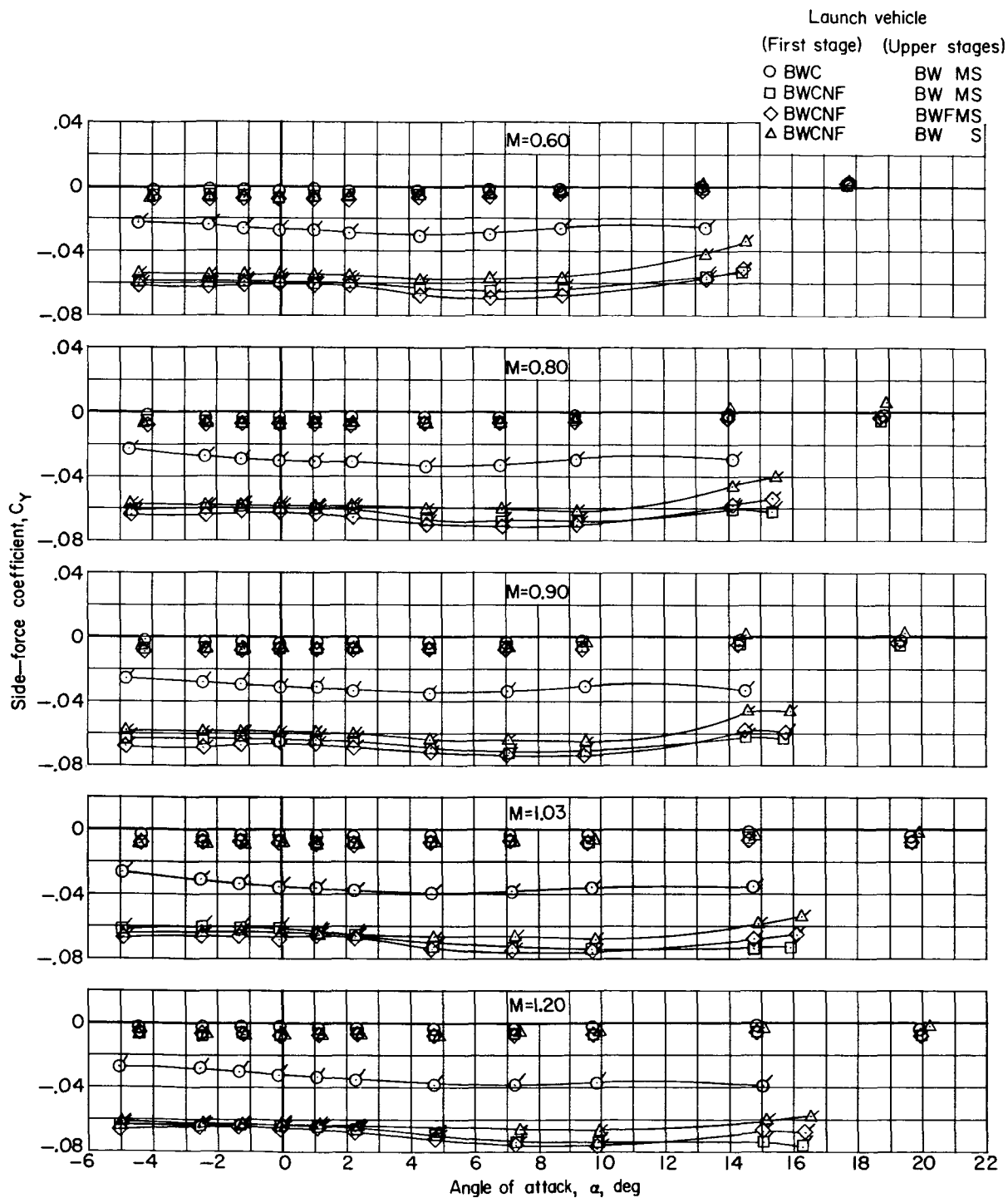


(b) Variation of yawing-moment coefficient with angle of attack.

Figure 15.- Continued.

# UNCLASSIFIED

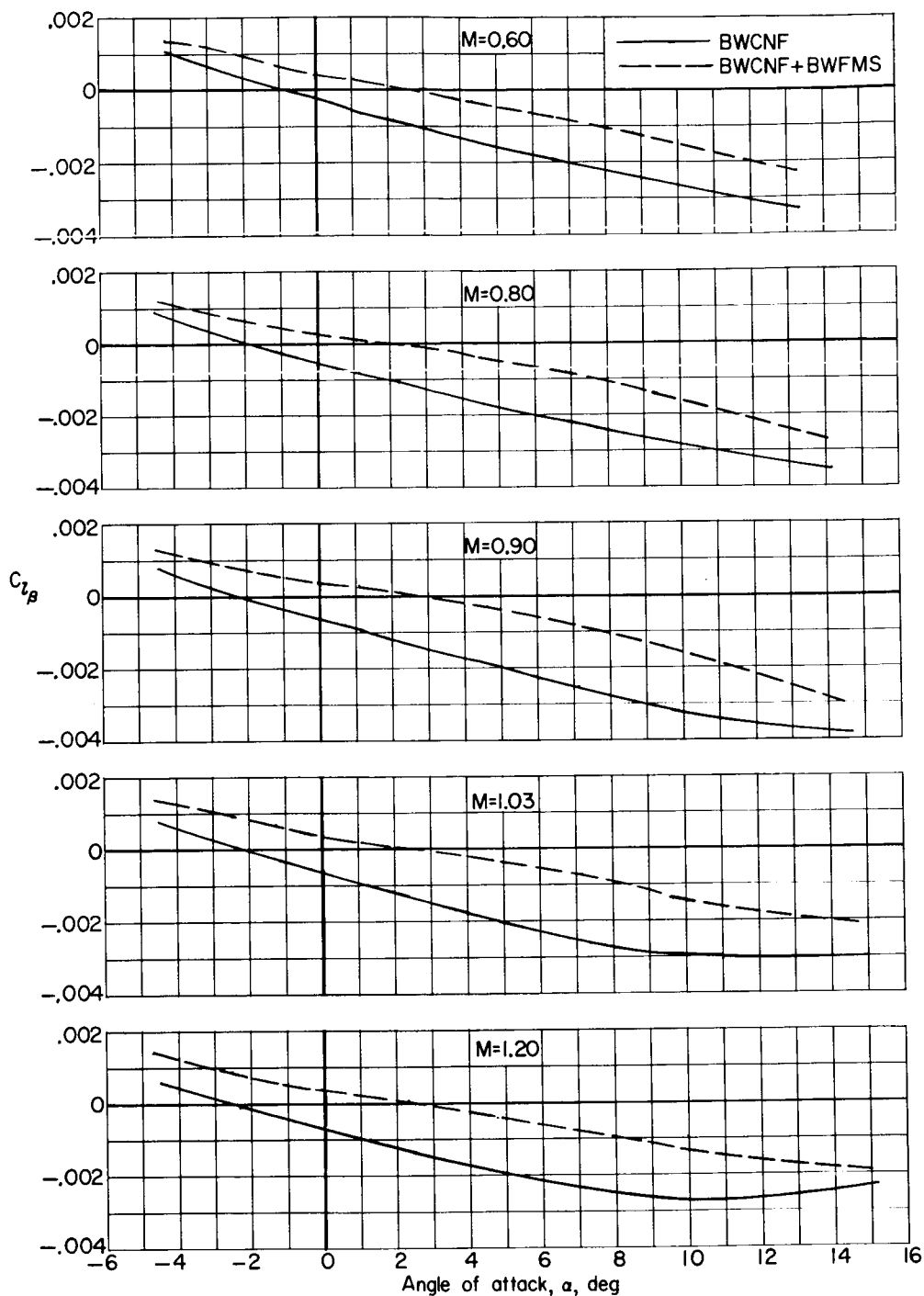
~~CONFIDENTIAL~~  
**UNCLASSIFIED**



(c) Variation of side-force coefficient with angle of attack.

Figure 15.- Concluded.

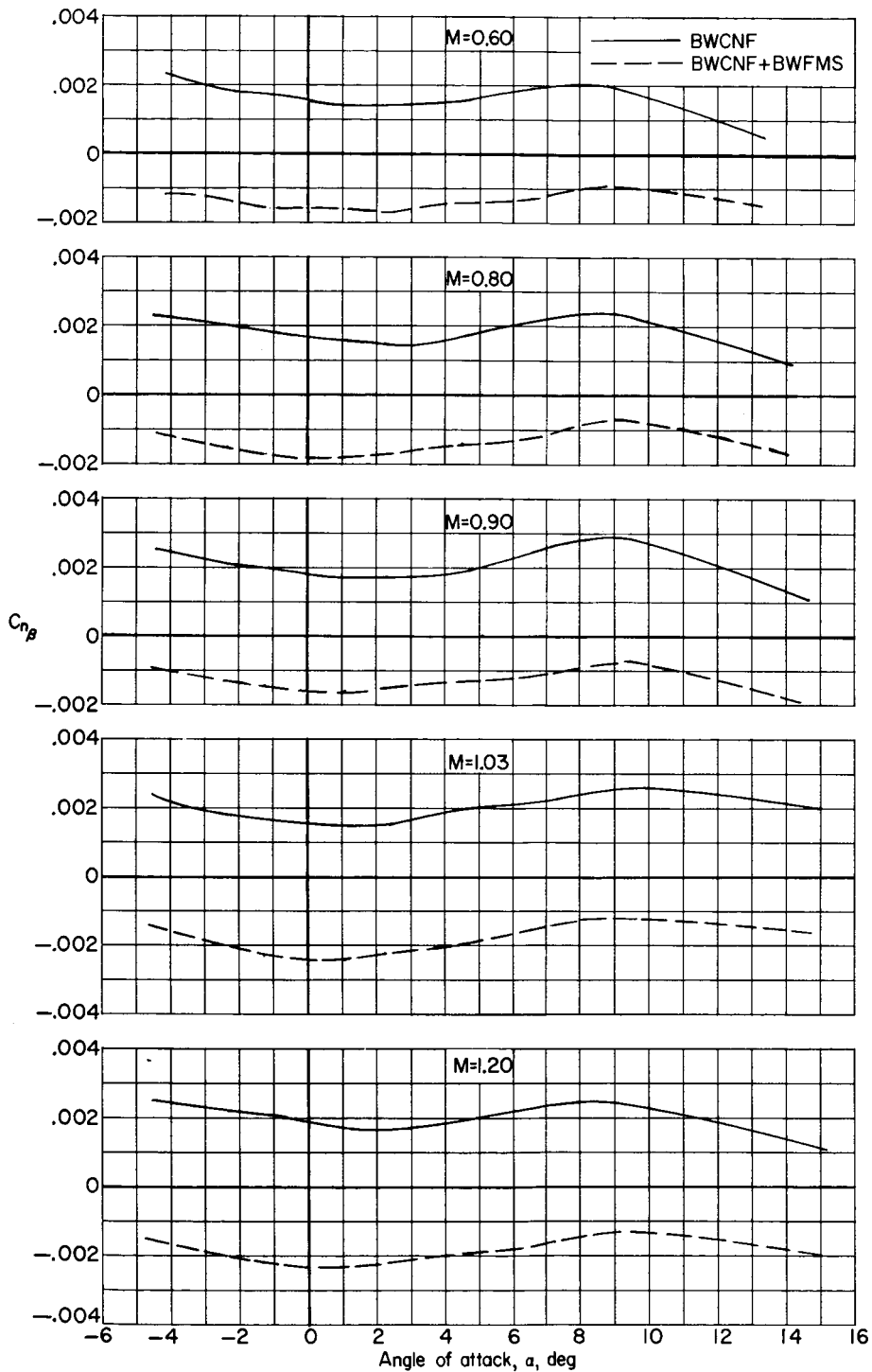
~~CONFIDENTIAL~~  
**UNCLASSIFIED**



(a) Variation of lateral-stability parameter with angle of attack.

Figure 16.- Variation with angle of attack of the lateral- and directional-stability parameters for the complete first stage and the complete launch vehicle.

~~CONFIDENTIAL~~  
UNCLASSIFIED



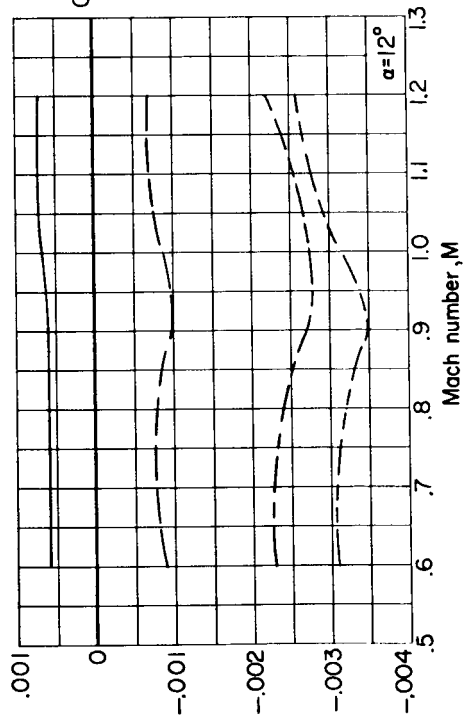
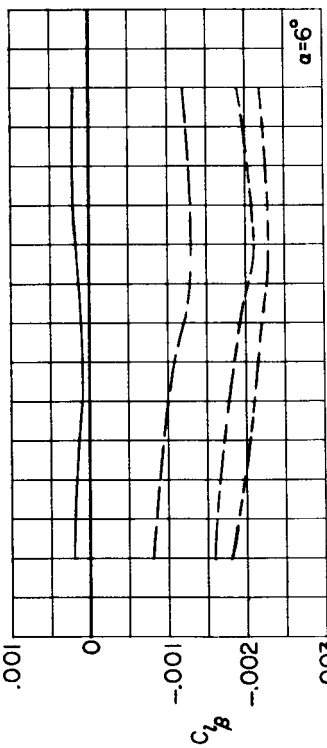
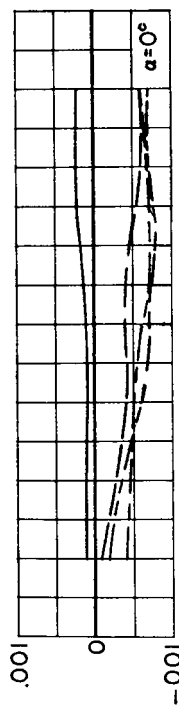
(b) Variation of directional-stability parameter with angle of attack.

Figure 16.- Concluded.

~~CONFIDENTIAL~~  
UNCLASSIFIED

## First-stage vehicle

— B  
 - - BW  
 - - BWC  
 - - BWCNF

Launch vehicle  
(First stage) (Upper stages)

— BWC BW MS  
 - - BWCNF BW MS  
 - - BWCNF BWFMS  
 - - BWCNF BW S

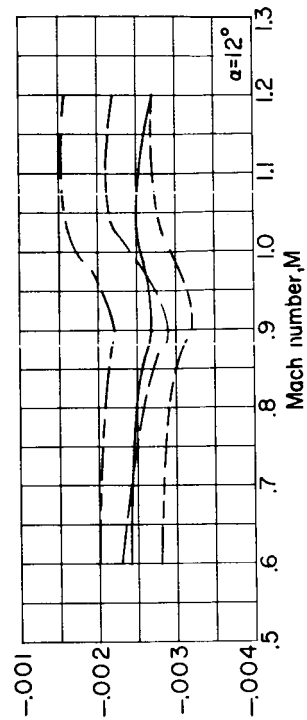
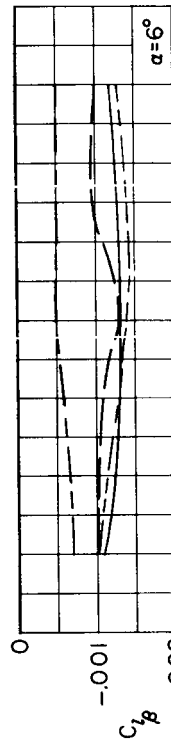
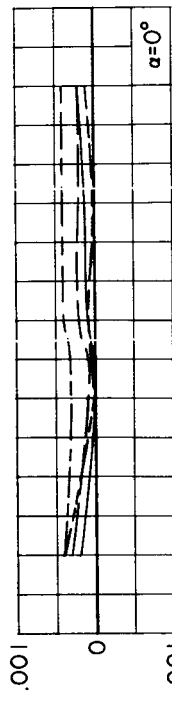


Figure 17.- Variation with Mach number of the lateral-stability parameters for several first-stage and launch configurations.  
 $\alpha = 0^\circ, 6^\circ, \text{ and } 12^\circ$ .

# UNCLASSIFIED

~~CONFIDENTIAL~~

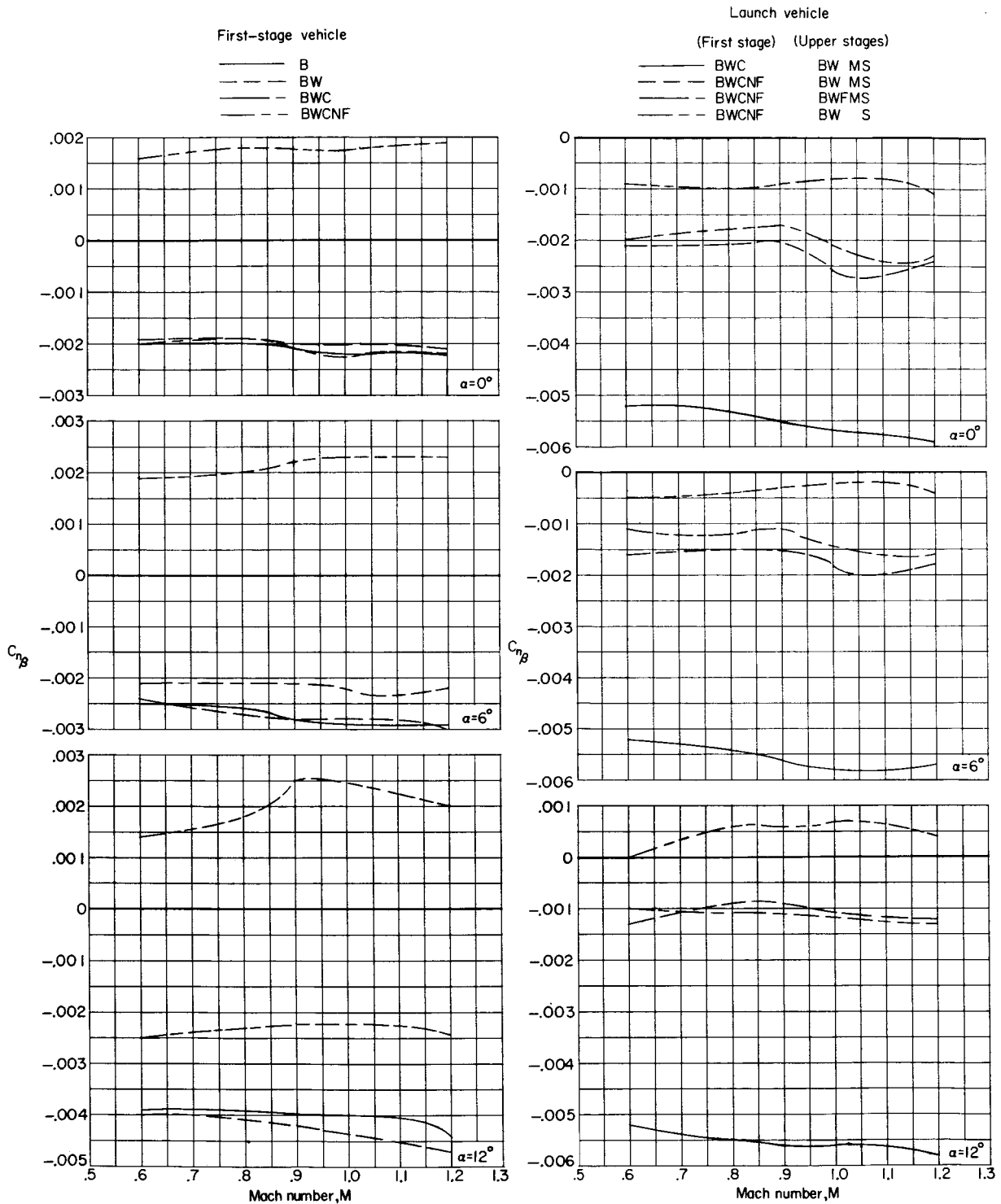


Figure 18.- Variation with Mach number of the directional-stability parameters for several first-stage and launch configurations.  $\alpha = 0^\circ$ ,  $6^\circ$ , and  $12^\circ$ .

~~CONFIDENTIAL~~

# UNCLASSIFIED



~~CONFIDENTIAL~~  
UNCLASSIFIED



*"The aeronautical and space activities of the United States shall be conducted so as to contribute . . . to the expansion of human knowledge of phenomena in the atmosphere and space. The Administration shall provide for the widest practicable and appropriate dissemination of information concerning its activities and the results thereof."*

—NATIONAL AERONAUTICS AND SPACE ACT OF 1958

## NASA SCIENTIFIC AND TECHNICAL PUBLICATIONS

**TECHNICAL REPORTS:** Scientific and technical information considered important, complete, and a lasting contribution to existing knowledge.

**TECHNICAL NOTES:** Information less broad in scope but nevertheless of importance as a contribution to existing knowledge.

**TECHNICAL MEMORANDUMS:** Information receiving limited distribution because of preliminary data, security classification, or other reasons.

**CONTRACTOR REPORTS:** Technical information generated in connection with a NASA contract or grant and released under NASA auspices.

**TECHNICAL TRANSLATIONS:** Information published in a foreign language considered to merit NASA distribution in English.

**TECHNICAL REPRINTS:** Information derived from NASA activities and initially published in the form of journal articles.

**SPECIAL PUBLICATIONS:** Information derived from or of value to NASA activities but not necessarily reporting the results of individual NASA-programmed scientific efforts. Publications include conference proceedings, monographs, data compilations, handbooks, sourcebooks, and special bibliographies.

*Details on the availability of these publications may be obtained from:*

SCIENTIFIC AND TECHNICAL INFORMATION DIVISION  
NATIONAL AERONAUTICS AND SPACE ADMINISTRATION  
Washington, D.C. 20546

UNCLASSIFIED

~~CONFIDENTIAL~~